Article | Received 6 January 2026; Revised 29 January 2026; Accepted 5 February 2026; Published 19 March 2026
https://doi.org/10.55092/aic20260002

Energy efficiency optimization of STAR-RIS-aided ISAC systems based on user fairness

Shuang Zhang, Wanming Hao* and Gangcan Sun

School of Electrical and Information Engineering, Zhengzhou University, Zhengzhou 450001, China

* Correspondence author; E-mail: iewmhao@zzu.edu.cn.

Highlights:

- Investigates STAR-RIS aided ISAC in near-field to optimize communication EE.
- Transforms non-convex problem via FP and AO algorithms under sensing constraints.
- Simulations confirm the proposed scheme's effectiveness in balancing user fairness and sensing.

Abstract: In this paper, the communication energy efficiency (EE) of simultaneously transmitting and reflecting reconfigurable intelligent surface (STAR-RIS) aided integrated sensing and communications (ISAC) systems underlying a near-field scenario is investigated, where the dual-functional base station (DFBS) serves multiple users and senses multiple targets simultaneously. To ensure user fairness, we formulate an optimization problem that maximizes the minimum (max-min) communication EE while satisfying the minimum target illumination power requirement, the maximum transmission power budget, and the hardware constraints of STAR-RIS under its three operation modes. The formulated max-min optimization problem exhibits non-convexity due to the high coupling among the optimization variables. So as to resolve this issue, the fractional programming is first leveraged to transform the objective function into a more tractable structure. Then, the original max-min problem is transformed into an equivalent maximization problem via introducing the auxiliary variable. Next, we propose an alternating optimization framework to decouple the newly reformulated maximization problem into several sub-problems, which are optimized iteratively until convergence. Finally, the outcomes from the simulations are executed to confirm the advantages and effectiveness of the schemes we have introduced.

Keywords: simultaneously transmitting and reflecting reconfigurable intelligent surface; near-field; integrated sensing and communication; max-min

1. Introduction

Among the myriad of groundbreaking technologies of sixth generation (6G), the integrated sensing and communication (ISAC) technology stands as a vital force, propelling the future of communications into uncharted territories of revolution [1]. This innovative paradigm fuses the realms of wireless communication

and radar perception into a seamless whole, transcending traditional boundaries to achieve a profound integration that redefines the capabilities of both domains. Through sharing spectrum resources and hardware platforms, ISAC technology integrates wireless communication and radar perception, realizes the deep integration of communication and sensing and fosters a synergy, thereby not only improving the system's efficiency but also elevating the overall performance, ushering in a new era of optimized resource utilization. As the global demand for spectrum resources continues to expand exponentially, fueled by the proliferation of diverse and sophisticated applications, the integration of communication and sensing functionalities has emerged as an inexorable trend [2]. This convergence addresses the pressing need for more intelligent and adaptable networks that can dynamically allocate resources, ensure seamless connectivity, and simultaneously provide advanced sensing capabilities. It can be anticipated that the development of ISAC technology will lay a solid foundation for intelligent networks in the era of 6G, promoting the development of wireless communication technology towards a more efficient, flexible and intelligent direction.

However, in practical applications, ISAC faces numerous challenges, such as high environmental dependency, high cost and power consumption, limited coverage range, and the existence of many coverage blind spots. Especially when applied to high-frequency broadband systems such as millimeter wave (mmWave) systems or terahertz (THz) systems, and owing to the transmission path loss, the propagation of these high-frequency signals is particularly susceptible to the influence of environmental obstacles, resulting in severe transmission losses, which leads to both the line-of-sight (LoS) path and the non-line-of-sight (NLoS) path being relatively weak, hindering reliable communication and sensing [3]. To resolve this issue, the current research hotspot is to combine reconfigurable intelligent surfaces (RIS) with ISAC, providing virtual LoS link gain through the deployment of RIS, thereby compensating for the transmission attenuation of ISAC signals [4,5].

1.1. Related works

Currently, significant research efforts have been devoted to the realm of joint transmit beamforming design for RIS-assisted ISAC systems [6–11]. Concretely, the authors [6] explored a radar-communication coexistence (RCC) system that deployed dual RIS, where one RIS was located adjacent to the base station (BS) to attenuate the interference directed towards the radar, while the other RIS was positioned close to users to fulfill the objective of eliminating radar interference. The communication signal-to-interference-plus-noise ratio (SINR) was optimized by employing an effective joint beamforming strategy for both the BS and RIS, while adhering to the constraints imposed by the radar SINR necessary for target detection and the total power limitations. The authors [7] further delved into an in-depth analysis of the implications of imperfect channel state information (CSI) and proposed a robust beamforming design for an RIS-assisted RCC system built upon this, ensuring facilitating efficient and reliable functioning of the RIS system amidst channel uncertainties and external interferences. The authors [8] considered a more realistic urban scenario where the direct link between BS and target/user is obscured, and the RIS was deployed to assist the BS in simultaneously performing radar detection and communication. Under this scenario, a novel RIS-assisted beamforming strategy was introduced. By taking into account the target size, the concept of ultimate detection resolution (UDR) based on target dimensions was proposed to evaluate the

target detection capability. Subsequently, under the constraint of meeting the minimum UDR requirement, the communication SNR was maximized. When the LoS link exists between the BS and the target, the virtual LoS path constructed by RIS can also be used to further enhance the sensing capability of the BS. For instance, the authors [9] studied a multi-user multiple-input single-output scenario, in which the total communication rate was maximized through jointly optimizing the BS transmit beamforming, radar receive filter and RIS reflection coefficients. The authors [10] addressed a more complex scenario with the presence of multi-path solid clutter interference. By utilizing an algorithm based on the alternating direction method of multipliers (ADMM) and majorization minimization (MM), the BS beamforming, BS receive filter, and RIS reflection coefficients were jointly designed while maximizing radar SINR under communication service quality and constant modulus constraints. In addition, when the BS conducts target sensing, the received echo signal will undergo four-link attenuation from the BS-RIS-target-RIS-BS path, significantly degrading the detection performance. To this end, the concept of hybrid RIS, which consists of passive reflective elements (REs) and active sensing elements (SEs), has been introduced. The active SEs collect echoes that are reflected from targets to facilitate angle estimation. In contrast to fully passive RIS, hybrid RIS substantially mitigate the path loss of echo signals by circumventing the attenuation associated with the RIS-BS link. For example, the authors [11] investigated a millimeter-wave communication system under this model and proposed a simultaneous beam training and sensing protocol to accommodate the actual millimeter-wave systems. Meanwhile, by analyzing the echo signals returned from the SEs, the RIS estimates the angular positions of nearby targets, and closed-form expressions are obtained for the achievable communication user rate as well as the Cramér–Rao lower bound of the target angle estimation.

Notably, the aforementioned researches typically presume that both the communication users and targets resided within the far-field region of BS or RIS. This is because, in a traditional ISAC system, the antenna array dimensions are relatively small due to the inherent size restrictions of the antennas, bringing about a small near-field range and thereby making the assumption of far-field plane waves appropriate [12]. Nevertheless, advancements in high-frequency communications have made it possible for BS to be equipped with ultra-large-scale antenna arrays or large intelligent surfaces [13,14], which broaden the array aperture and shorten the wavelength, causing the near-field region of BS or RIS to expand rapidly, thereby, there is a heightened likelihood of communication and sensing occurring within the near-field. In this scenario, the far-field plane wave channel model will no longer be applicable, necessitating the adoption of a near-field spherical wave channel model, which offers a more reasonable and applicable approach [15–17]. As a result, a disparity arises between current RIS-assisted ISAC designs that are premised on the far-field assumption and the actual wireless environments.

Furthermore, the reflective-only nature of RIS necessitates the assumption that communication users or sensing targets must be situated on the same side as both the RIS and BS, limiting coverage to only half of the space and severely constraining the deployment flexibility of RIS in practical systems. To address this, the novel concept of simultaneously transmitting and reflecting reconfigurable intelligent surface (STAR-RIS) has emerged, which offers the capability for the concurrent reflection and transmission of signals, enabling 360-degree full-space coverage [18]. Given the significant advantages of STAR-RIS, substantial research initiatives have been undertaken to leverage STAR-RIS for diverse goals within the realm of wireless

communication [19–21]. However, investigations into STAR-RIS-enabled ISAC systems remain in the preliminary stages [22–25].

1.2. Main contributions

Through our extensive search, the application of STAR-RIS to near-field ISAC systems has yet to thoroughly delve into the research thus far amidst the growing trend of expanding the scope of near-field region. It is imperative to design transmission strategies for the STAR-RIS-aided near-field ISAC systems. Hence, inspired by the above discussions, the joint beamforming optimization design in the STAR-RIS-aided a downlink near-field ISAC system is investigated in this paper to fill the research gap. Overall, the primary contributions are outlined as follows:

- In this paper, we explore the potential of deploying STAR-RIS in a downlink near-field ISAC system for the first time, wherein the dual-functional BS (DFBS) transmits the dual-functional signals to provide communication services to multiple users while performing multiple target sensing, and both the users and target located within the near-filed area of STAR-RIS. For the considered system, we analyze three modes of STAR-RIS [20,26], namely, the energy splitting (ES) mode, mode switching (MS) mode, and time switching (TS) mode. Under these three modes, we explore the joint beamforming optimization design of DFBS and STAR-RIS, with the intention of maximizing the minimum (max-min) energy efficiency (EE) of communication users while satisfying the target minimum illumination power, the DFBS maximum transmission power, and the hardware constraints of STAR-RIS.
- Since the objective function is in the form of a non-smooth fraction and has the characteristic of strong coupling, the direct solution to the formulated problem poses significant challenges and difficulties. To resolve this issue, we first leverage the fractional programming (FP) method to convert the original problem into a subtractive structure that is more tractable. Next, by bringing in an auxiliary variable representing the minimum communication user EE, the formed max-min optimization problem is reformulated into an equivalent maximization optimization problem, thereby eliminating the non-smoothness of the max-min objective function. Subsequently, the newly rewritten maximization optimization problem is addressed based on the alternating optimization (AO) framework, where the optimization problem is decomposed into several sub-problems which are alternately resolved until convergence.
- Hereafter, we introduce the solutions under ES and MS modes, and then present the solution under TS mode. Specifically, for the former two modes, the optimization problem can be decomposed into two sub-problems, *i.e.*, the DFBS transmit beamforming optimization sub-problem and the STAR-RIS transmission coefficients (TCs) and reflection coefficients (RCs) optimization sub-problem. By fixed STAR-RIS TCs/RCs, the optimization sub-problem for DFBS can be solved based on the semi-definite relaxation (SDR) and semi-definite programming (SDP) algorithms. By fixed DFBS transmit beamforming, a penalty-based algorithm for ES mode and an extended penalty-based algorithm for MS mode are proposed to optimize the STAR-RIS TCs/RCs. For the TS mode, due to its inclusion of the time factors, its decomposed optimization sub-problems not only encompass the DFBS optimization and STAR-RIS TCs/RCs optimization sub-problems but

also include an additional optimization sub-problem of the time factors. The first two sub-problems can be solved using the similar solution as in ES mode, while the optimization of the time factors, with other variables fixed, we show that it is a standard linear optimization problem that we can adopt the CVX tools to solve directly.

- Finally, extensive numerical experiments are carried out to illustrate the benefits of deploying STAR-RIS within the near-field ISAC system, as well as to confirm the convergence and efficacy of the algorithms we have proposed. The results indicate that our proposed schemes utilizing the ES mode can own the highest system performance.

1.3. Notation

Notations: Throughout this paper, the following notations are utilized for clarity. Typically, bold lowercase letters represent column vectors, and bold uppercase letters signify matrices. For a vector c, $\|c\|_F$ and $\|c\|$ indicates the Euclidean-norm and F-norm of the input vector, respectively, diag(c) refers to the diagonal operation and $[c]_i$ is the i-th value of c. For a matrix $\mathbf{R}$, $\mathbf{R} \succeq 0$ represents the semi-positive definiteness of $\mathbf{Q}$, $[\mathbf{Q}]_{i,j}$ indicates the i-th row and j-th column elements of $\mathbf{Q}$, Rank($\mathbf{Q}$), Tr($\mathbf{Q}$), respectively, indicate the rank and the trace of $\mathbf{Q}$, $(\mathbf{Q})^T$ and $(\mathbf{Q})^H$ respectively denote the transpose and the conjugate-transpose of $\mathbf{Q}$, and diag($\mathbf{Q}$) refers to obtain the diagonal elements from $\mathbf{Q}$. For a complex variable e, diag(e) refers to forming a diagonal matrix based on e and $|e|$ is the modulus of $|e|$. $\mathbb{C}^{m\times n}$ and $\mathbb{R}^{m\times n}$ indicate the complex space and the real space with a dimension of $m \times n$, respectively. $\mathbb{E}\{\cdot\}$ refers to the statistical expectation vaule. Besides, $\mathbf{I}_N$ denotes the $N \times N$ identity matrix. In addition, we have summarized the main symbols and their corresponding means in Table 1 to provide a better reading experience and facilitate understanding.

Table 1. Notations.

Notation	Description
M	The number of DFBS transmit/receive antennas
N	The number of STAR-RIS elements
K/Q	The total number of users and targets
K_r/K_t	The number of users at reflection space and transmission space
Q_r/Q_t	The number of targets at reflection space and transmission space
Φ_r/Φ_t	The reflection and transmission coefficient matrices of STAR-RIS
φ_r/φ_t	Equivalent STAR-RIS reflection and transmission coefficient vectors
x	Transmission signal at DFBS
s_k/$\mathbf{d}$	Communication signal and sensing signal
ω_k	Beamforming vector for the k-th user
$\mathbf{G}$	Channel from DFBS to STAR-RIS
$\mathbf{h}_k$	Channel from STAR-RIS to the k-th user
$\mathbf{h}_q$	Channel from STAR-RIS to the q-th target
n_k/n_q	Complex AWGN (Additive White Gaussian Noise) of the k-th user and the q-th target
σ_k^2/σ_q^2	Variances of n_k and n_q
τ_q	The sensing illumination power requirement for the q-th target
$P^{\max}$	The power budget at DFBS

2. System model and problem formulation

In this section, the system model for the considered STAR-RIS-aided near-field ISAC systems is first given, and then a max-min fairness optimization problem of communication EE is formulated.

2.1. System model

A near-field downlink ISAC system is investigated, in which the STAR-RIS assists the DFBS sensing Q targets and communicating with K users simultaneously. Herein, we postulate that the DFBS is furnished with M antennas (collectively denoted by the set $\mathscr{M}$), arranged in a uniform linear arrays (ULAs) configuration, and the STAR-RIS incorporates N transmission & reflection elements (represented by the set $\mathscr{N}$). As illustrated in Figure 1, it is presumed that obstacles intervene between the DFBS and the targets as well as users, and due to the high absorption and susceptibility to blockage of the signals causes the LoS links to be easily obstructed, which is a common occurrence in systems that utilize the high frequencies. As such, STAR-RIS is deployed near target/user to create virtual LoS paths, enabling DFBS to both serve users and perform target sensing. Based on this, the channels between STAR-RIS and users/targets are considered the near-field channels, while the channels between STAR-RIS and DFBS are relatively far, and the far-field channel model can be applied to the DFBS-STAR-RIS link. Besides, via deploying the STAR-RIS, the coverage region is partitioned into two separate halves: the reflection sapce (referred to as 'r-space') and the transmission space (known as 't-space'). Without loss of generality, users and targets located in the r-space are referred to as r-users and r-targets, respectively, which are indexed by the sets $\mathscr{K}_r \triangleq \{1,2,\ldots,K_r\}/\mathscr{Q}_r \triangleq \{1,2,\ldots,Q_r\}$, while users/targets that placed in the transmission space known as the t-user/t-target and can be denoted by the set of $\mathscr{K}_t \triangleq \{1,2,\ldots,K_t\}/\mathscr{Q}_t \triangleq \{1,2,\ldots,Q_t\}$, and we have $K_r + K_t = K/Q_r + Q_t = Q$. Additionally, proposed system employs advanced self-interference cancellation techniques that include both passive suppression (via antenna isolation and spatial separation) and active cancellation (using digital signal processing). To this end, we propose the hypothesis of perfect self-interference cancellation, building on previous works such as [27–29].

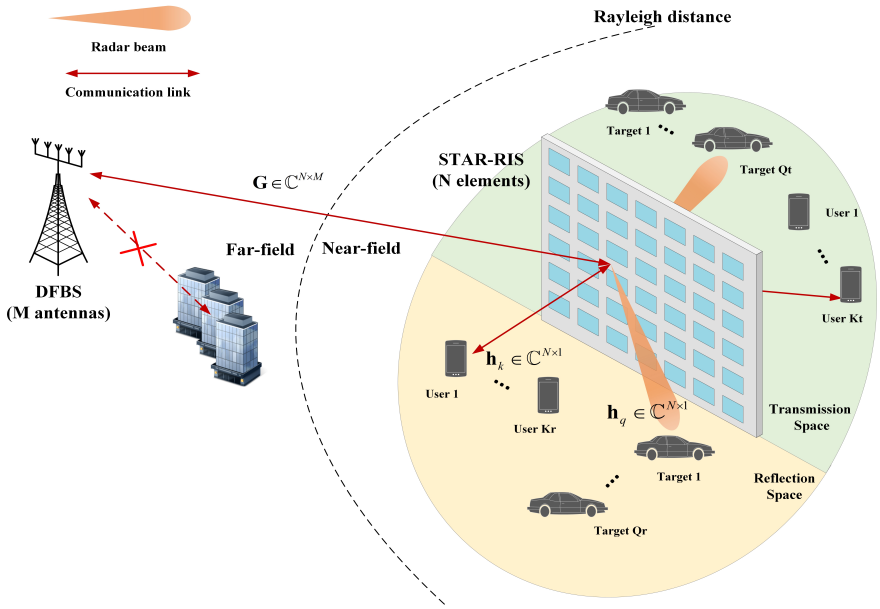

Figure 1. STAR-RIS-aided near-field ISAC system model.

For STAR-RIS, we define $\Phi_t \in \mathbb{C}^{N\times N}$ and $\Phi_r \in \mathbb{C}^{N\times N}$ be the TCs ($i=t$) matrix and RCs ($i=r$) matrix, respectively, which given by:

$$\Phi_t = \mathrm{diag}([\beta_{t,1}e^{j\phi_{t,1}}, \beta_{t,2}e^{j\phi_{t,2}}, \ldots, \beta_{t,N}e^{j\phi_{t,N}}]^T), \tag{1}$$

$$\Phi_r = \mathrm{diag}([\beta_{r,1}e^{j\phi_{r,1}}, \beta_{r,2}e^{j\phi_{r,2}}, \ldots, \beta_{r,N}e^{j\phi_{r,N}}]^T), \tag{2}$$

where $\phi_{i,n} \in (0, 2\pi]$ and $\beta_{i,n} \in [0,1], \forall i \in \{t,r\}$, respectively, denote the phase-shift coefficient and amplitude coefficient of RCs/TCs of the n-th STAR-RIS element. For the sake of simplicity in description, we define $\varphi_i = [\beta_{i,1}e^{j\phi_{i,1}}, \beta_{i,2}e^{j\phi_{i,2}}, \ldots, \beta_{i,N}e^{j\phi_{i,N}}]^T \in \mathbb{C}^{N\times 1}, \forall i \in \{t,r\}$ for further use. Besides, each STAR-RIS element $n, \forall n \in \mathcal{N}$, boasts the capability of individually modulating its phase-shift coefficients $\{\phi_{r,n}, \phi_{t,n}\}$, whereas the amplitude coefficients $\{\beta_{r,n}, \beta_{t,n}\}$ are inherently constrained by the principle of energy conservation, fostering a coupling relationship between them, specifically adhering to the condition $\beta_{r,n}^2 + \beta_{t,n}^2 = 1$.

Compared to conventional RIS, there are three modes typically adopted by STAR-RIS, *i.e.*, ES, MS, and TS. Here is a brief overview of the three modes:

- ES mode: Each STAR-RIS element is operated in transmission and reflection state (T&R state) simultaneously, dividing the incident signal into transmissive and reflective signals. Due to the law of conservation of energy, the transmission/reflection amplitude coefficient of the n-th STAR-RIS element should satisfy $\mathscr{A}^{\mathrm{ES}} \triangleq \{\beta_{t,n}, \beta_{r,n} \mid \beta_{t,n}, \beta_{r,n} \in [0,1]; \beta_{t,n} + \beta_{r,n} = 1\}$. The ES mode offers the highest flexibility in design.
- MS mode: Each STAR-RIS element is operated either in full T state or full R state, but not both simultaneously. Thus, the transmission/reflection amplitude coefficient of the n-th STAR-RIS element should satisfy $\mathscr{A}^{\mathrm{MS}} \triangleq \{\beta_{t,n}, \beta_{r,n} \mid \beta_{t,n}, \beta_{r,n} \in \{0,1\}; \beta_{t,n} + \beta_{r,n} = 1\}$. In comparison to the ES mode, the MS mode cannot attain the same level of beam gain, however, it is comparatively simpler to implement.
- TS mode: The STAR-RIS periodically switches all elements between T state (refers to as T period) and R state (refers to as R period) in different orthogonal time slots. Let $0 \le \lambda^t \le 1$ and $0 \le \lambda^r \le 1$ stands for the percentage of execution time allocated to T periods and R periods, respectively, where $\lambda^t + \lambda^r = 1$. Therefore, the transmission/reflection amplitude coefficient of the n-th STAR-RIS element should satisfy $\mathscr{A}^{\mathrm{TS}} \triangleq \{\beta_{\mathrm{t},n}, \beta_{r,n} \mid \beta_{t,n} = 1, \beta_{r,n} = 1\}$. Under this mode, the TCs & RCs design for STAR-RIS is relatively simple. However, precise synchronization in the time domain is essential for accurate implementation of this mode.

2.2. *Channel model*

As shown in Figure 2, in the far-field scenario, the channel is modeled under the assumption of a planar wavefront. In near-field scenarios, it is necessary to model the channel under the assumption of spherical wavefront. Assuming the channel wavelength is λ and the distance between adjacent elements of STAR-RIS is d_s, thus, the aperture of STAR-RIS is $D = (N-1)d_s$ and the Rayleigh distance can be calculated as $2D^2/\lambda$ [30,31]. Note that, In our paper, to enable designing the beamforming matrix and the STAR-RIS reflection & transmission coefficients, we assume that the CSI is known a priori perfectly for DFBS. In practice, although the passive nature of RISs makes the channel estimation challenging, many

effective estimation methods [32–35] for conventional RIS-assisted systems have been proposed to tackle this issue, which can also be easily applied to STAR-RISs. For example, the TS mode of STAR-RIS can be utilized to achieve channel estimation. In TS mode, the existing channel estimation methods can be used to continuously estimate the CSI of users at the transmission and reflection ends. Subsequently, DFBS can apply parallel factor decomposition methods to unfold cascaded channel patterns [36], thereby estimating the channels from BS to STAR-RIS and from STAR-RIS to each user, respectively.

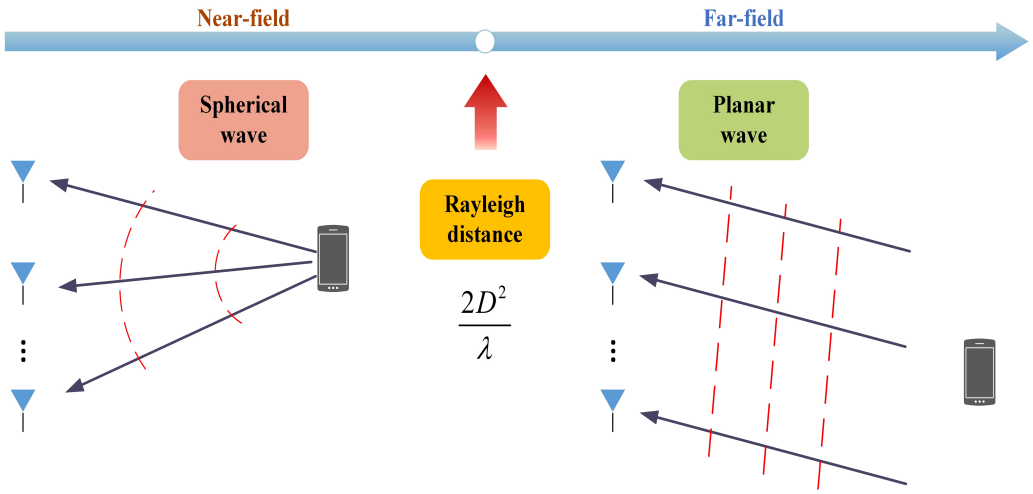

Figure 2. A comparison for the far-field and the near-field propagation.

2.2.1. The far-field channel model

The DFBS is located in the far-field region of STAR-RIS, its channel follows the plane wave model. Assuming the channel between DFBS and STAR-RIS is $\mathbf{G} \in \mathbb{C}^{N\times M}$, and we have:

$$\mathbf{G} = \sqrt{\frac{MN}{L}} \sum_{l=1}^{L} \gamma_l \mathbf{a}^{\text{far}}_{\text{STAR-RIS}}\left(\tilde{\vartheta}_l\right) \mathbf{a}^{H}_{\text{DFBS}}\left(\hat{\vartheta}_l\right), \tag{3}$$

where, γ_l is the complex channel gain, $\tilde{\vartheta}_l$ represents the arrive of angle associated with STAR-RIS, and $\hat{\vartheta}_l$ represents the departure of angle associated with DFBS. We assume that both DFBS and STAR-RIS are ULA, and their array steering vectors are respectively expressed as:

$$\mathbf{a}_{\text{DFBS}}\left(\hat{\vartheta}_l\right) = \left[1, e^{\frac{j2\pi d_b \sin(\hat{\vartheta}_l)}{\lambda}}, \cdots, e^{\frac{j2\pi(M-1) d_b \sin(\hat{\vartheta}_l)}{\lambda}}\right]^T, \tag{4}$$

$$\mathbf{a}^{\text{far}}_{\text{STAR-RIS}}\left(\tilde{\vartheta}_l\right) = \left[1, \cdots, e^{\frac{j2\pi(N-1) d_s \sin(\tilde{\vartheta}_l)}{\lambda}}\right]^T, \tag{5}$$

where $d_b = \lambda/2$ indicates the interval between DFBS antennas.

2.2.2. The near-field channel model

We assume that the users and targets within the near-field region of STAR-RIS. By adopting a 3D coordinate system, without loss of generality, we consider the coordinate origin at the center of STAR-RIS, and the coordinate of the STAR-RIS n-th element can be denoted by $\mathbf{s}_n = [nd_s, 0, 0]^T$. We define r_k and θ_k respectively are the distance and angle between the k-th communication user and the STAR-RIS center. Thus, the coordinate of the k-th user is calculated by $\mathbf{r}_k = [r_k \cos\theta_k, r_k \sin\theta_k, 0]^T$, and the distance from the

n-th STAR-RIS element to the k-th user is represented as $r_n^k(r_k,\theta_k)=\|\mathbf{r}_k-\mathbf{s}_n\|=\sqrt{r_k^2+n^2d_s^2-2r_k n d_s\cos\theta_k}$. Let $\mathbf{h}_k\in\mathbb{C}^{N\times 1}$ be the near-field channel between the STAR-RIS and the k-th user which is expressed as:

$$\mathbf{h}_k=\left[h^k_{-\tilde{N}}(r_k,\theta_k),\ldots,h^k_n(r_k,\theta_k),\ldots,h^k_{\tilde{N}}(r_k,\theta_k)\right]^T, \tag{6}$$

where $h^k_n(r_k,\theta_k)=\gamma_k e^{-j\frac{2\pi}{\lambda}\left(r^k_n(r_k,\theta_k)-r_k\right)}$ denotes the channel between the n-th STAR-RIS element and the k-th user, and $\tilde{N}=\lfloor N/2\rfloor$. $\gamma_k=\frac{\sqrt{\lambda}}{\sqrt{4\pi r_k}}$ is the complex channel gain [37].

Similarly, the near-field channel between the STAR-RIS and the q-th target can be calculated as:

$$\mathbf{h}_q=\left[h^q_{-\tilde{N}}(r_q,\theta_q),\ldots,h^q_n(r_q,\theta_q),\ldots,h^q_{\tilde{N}}(r_q,\theta_q)\right]^T, \tag{7}$$

where $h^q_n(r_q,\theta_q)=\gamma_q e^{-j\frac{2\pi}{\lambda}\left(r^q_n(r_q,\theta_q)-r_q\right)}$ denotes the channel between the n-th STAR-RIS element and the q-th target, and $\gamma_q=\frac{\sqrt{\lambda}}{\sqrt{4\pi r_q}}$.

2.3. *Downlink transmit signal model*

DFBS transmits the combined signal $x[t]\in\mathbb{C}^{M\times 1}$:

$$x[t]=\sum_{k\in\mathscr{K}}\omega_k s_k[t]+\mathbf{d}[t], \tag{8}$$

where $s_k[t]$ and $\omega_k\in\mathbb{C}^{M\times 1}$ refers to the information-bearing symbol at the time slot t for the k-th user, and $w_k\in\mathbb{C}^{M\times 1}$ is the corresponding communication beamforming for the k-th user. $\mathbf{d}[t]\in\mathbb{C}^{M\times 1}$ denotes the dedicated sensing signal. Specifically, we assume that $s_k[t]\sim\mathscr{CN}(0,1),\mathbb{E}\{s_k[t]s_{k'}[t]\}=0,k\neq k',\forall k,k'\in\mathscr{K}$ and $\mathbf{d}[t]\sim\mathscr{C}N(0,\mathbf{R}_{\mathrm{d}})$, where $\mathbf{R}_{\mathrm{d}}=\mathbb{E}\left[\mathbf{d}[t]\mathbf{d}^H[t]\right]\succeq\mathbf{0}$. In addition, to mitigate potential mutual interference between sensing and communication processes, it is assumed that the communication signals and sensing signals are inherently independent of each other. The power consumption of the transmitted signals with STAR-RIS ES/MS mode can then be expressed as:

$$\begin{aligned}P_T^{\mathrm{ES/MS}}&=\sum_{k\in\mathscr{K}}\|\omega_k\|^2+\mathrm{Tr}(\mathbf{R}_{\mathrm{d}})\\&=\sum_{k\in\mathscr{K}}\omega_k\omega_k^H+\mathrm{Tr}(\mathbf{R}_{\mathrm{d}})=\mathrm{Tr}\left(\sum_{k\in\mathscr{K}}\mathbf{W}_k+\mathbf{R}_{\mathrm{d}}\right).\end{aligned} \tag{9}$$

While for STAR-RIS TS mode, due to the existence of the time factor λ_i, the power consumption of the transmitted signals is:

$$P_T^{\mathrm{TS}}=\lambda^t\,\mathrm{Tr}\left(\sum_{k\in\mathscr{K}_t}\mathbf{W}_k\right)+\lambda^r\,\mathrm{Tr}\left(\sum_{k\in\mathscr{K}_r}\mathbf{W}_k\right)+\mathrm{Tr}(\mathbf{R}_{\mathrm{d}}). \tag{10}$$

For notational simplicity, we define $\mathbf{W}_k=\omega_k\omega_k^H\in\mathbb{C}^{M\times M}$, where $\mathbf{W}_k\succeq\mathbf{0}$ and $\mathrm{Rank}(\mathbf{W}_k)=1$. Note that since the CSI remains unchanged in one frame, and the operations are the same for each time slot, without loss of generality and for notational convenience, we omit the time index in the following description of our paper.

2.3.1. Communication model

The received signal at the k-th user can be written as:

$$y_k = \mathbf{h}_k^H \Phi_i \mathbf{G} x + \mathbf{n}_k = \underbrace{\mathbf{h}_k^H \Phi_i \mathbf{G} \omega_k s_k}_{\text{desired signal}} + \underbrace{\mathbf{h}_k^H \Phi_i \mathbf{G} \sum_{j \in \mathcal{K}, j \neq k} \omega_j s_j}_{\text{inter-user interference}} + \underbrace{\mathbf{h}_k^H \Phi_i \mathbf{G} \mathbf{d}}_{\text{sensing interference}} + \mathbf{n}_k, \forall i \in \{t, r\}, \tag{11}$$

where, $n_k \sim \mathscr{C}N\left(0, \sigma_k^2\right)$ denotes the complex AWGN of the k-th user with zero mean and variances σ_k^2.

Considering the fact that $\tilde{\mathbf{h}}_k = \mathbf{h}_k^H \Phi_i \mathbf{G} = \varphi_i^H \operatorname{diag}\left(\mathbf{h}_k^H\right) \mathbf{G} = \varphi_i^H \mathbf{H}_k \in \mathbb{C}^{1 \times M}$, where $\mathbf{H}_k = \operatorname{diag}\left(\mathbf{h}_k^H\right) \mathbf{G} \in \mathbb{C}^{N \times M}$ can be seen as the equivalent cascaded channel from DFBS through STAR-RIS to user k. For the sake of simplicity, let $\Psi_i = \varphi_i \varphi_i^H \in \mathbb{C}^{N \times N}, \forall i \in \{t, r\}$, where $\Psi_i \succeq \mathbf{0}$ and $\operatorname{Rank}\left(\Psi_i\right) = 1$.

For ES and MS modes, the SINR of the k-th user is:

$$\begin{aligned} \mathrm{SINR}_k^{\mathrm{ES/MS}} &= \frac{\left|\mathbf{h}_k^H \Phi_i \mathbf{G}_k\right|^2}{\sum_{j \in \mathcal{K}, j \neq k} \left|\mathbf{h}_k^H \Phi_i \mathbf{G} \omega_j\right|^2 + \left|\mathbf{h}_k^H \Phi_i \mathbf{G} \mathbf{d}\right|^2 + \sigma_k^2} \\ &= \frac{\left|\tilde{\mathbf{h}}_k \omega_k\right|^2}{\sum_{j \in \mathcal{K}, j \neq k} \left|\tilde{\mathbf{h}}_k \omega_j\right|^2 + \left|\tilde{\mathbf{h}}_k \mathbf{d}\right|^2 + \sigma_k^2} \\ &= \frac{\left|\varphi_i^H \mathbf{H}_k \omega_k\right|^2}{\sum_{j \in \mathcal{K}, j \neq k} \left|\varphi_i^H \mathbf{H}_k \omega_j\right|^2 + \left|\varphi_i^H \mathbf{H}_k \mathbf{d}\right|^2 + \sigma_k^2} \\ &= \frac{\varphi_i^H \mathbf{H}_k \mathbf{W}_k \mathbf{H}_k^H \varphi_i}{\varphi_i^H \mathbf{H}_k \mathbf{J}_k^{\mathrm{ES/MS}} \mathbf{H}_k^H \varphi_i + \sigma_k^2} \\ &= \frac{\operatorname{Tr}\left(\mathbf{W}_k \mathbf{H}_k^H \Psi_i \mathbf{H}_k\right)}{\operatorname{Tr}\left(\mathbf{J}_k^{\mathrm{ES/MS}} \mathbf{H}_k^H \Psi_i \mathbf{H}_k\right) + \sigma_k^2}, \forall i \in \{t, r\}, \end{aligned} \tag{12}$$

where $\mathbf{J}_k^{\mathrm{ES/MS}} = \sum_{j \in \mathcal{K}, j \neq k} \mathbf{W}_j + \mathbf{R}_{\mathrm{d}} = \sum_{j \in \mathcal{K}} \mathbf{W}_j + \mathbf{R}_{\mathrm{d}} - \mathbf{W}_k$, and the achievable rate corresponding to the k-th user is:

$$R_k^{\mathrm{ES/MS}} = \log_2\left(1 + \mathrm{SINR}_k^{\mathrm{ES/MS}}\right). \tag{13}$$

For TS mode, the STAR-RIS operates in T mode or R mode in time-division manner, thus eliminating user interference in different spaces. The SINR of the k-th user at t/r-space is:

$$\begin{aligned} \mathrm{SINR}_{k,i}^{\mathrm{TS}} &= \frac{\left|\tilde{\mathbf{h}}_k \omega_k\right|^2}{\sum_{j \in \mathcal{K}_i, j \neq k} \left|\tilde{\mathbf{h}}_k \omega_j\right|^2 + \left|\tilde{\mathbf{h}}_k \mathbf{d}\right|^2 + \sigma_k^2} \\ &= \frac{\left|\varphi_i^H \mathbf{H}_k \omega_k\right|^2}{\sum_{j \in \mathcal{K}_i, j \neq k} \left|\varphi_i^H \mathbf{H}_k \omega_j\right|^2 + \left|\varphi_i^H \mathbf{H}_k \mathbf{d}\right|^2 + \sigma_k^2} \\ &= \frac{\varphi_i^H \mathbf{H}_k \mathbf{W}_k \mathbf{H}_k^H \varphi_i}{\varphi_i^H \mathbf{H}_k \mathbf{J}_k^{\mathrm{TS}} \mathbf{H}_k^H \varphi_i + \sigma_k^2} \\ &= \frac{\operatorname{Tr}\left(\mathbf{W}_k \mathbf{H}_k^H \Psi_i \mathbf{H}_k\right)}{\operatorname{Tr}\left(\mathbf{J}_k^{\mathrm{TS}} \mathbf{H}_k^H \Psi_i \mathbf{H}_k\right) + \sigma_k^2}, \forall i \in \{t, r\}, \end{aligned} \tag{14}$$

where $\mathbf{J}_k^{\mathrm{TS}} = \sum_{j \in \mathcal{K}_i, j \neq k} \mathbf{W}_j + \mathbf{R}_{\mathrm{d}} = \sum_{j \in \mathcal{K}_i} \mathbf{W}_j + \mathbf{R}_{\mathrm{d}} - \mathbf{W}_k, \forall i \in \{t, r\}$. The corresponding achievable rate

can be expressed as:

$$R_{k,i}^{\mathrm{TS}} = \lambda^i \log_2\left(1+\mathrm{SINR}_{k,i}^{\mathrm{TS}}\right), \forall i \in \{t,r\}. \tag{15}$$

Note that, for Equations (14) and (15), if user k located in r-space, there has $i=r$, and vice versa.

We adopt the linear power model as in [38,39], where the total power consumption at the k-th user includes the transmit power and the total circuit power as follows:

$$P_k^{\mathrm{total}} = \frac{1}{\varepsilon}\mathrm{Tr}\left(\mathbf{W}_k+\mathbf{R}_{\mathrm{d}}\right)+P_C, \tag{16}$$

where $\varepsilon \in [0,1]$ is the PA efficiency. The total circuit power consumption P_C can be calculated as $P_C = P_{DFBS}+NP_{STAR-RIS}+P_{User}$, where $P_{DFBS}, P_{STAR-RIS}$ and P_{User} refer to the hardware-dissipated power consumed by DFBS, each STAR-RIS element and user, respectively. Thus, the EE of the k-th user is defined as the ratio of the k-th user rate to its total power consumption, which can be expressed as:

$$EE_k^{\mathrm{ES/MS/TS}} = \begin{cases} \frac{R_k^{\mathrm{ES/MS}}}{\frac{1}{\varepsilon}\mathrm{Tr}(\mathbf{W}_k+\mathbf{R}_{\mathrm{d}})+P_C}, \\ \frac{R_{k,i}^{\mathrm{TS}}}{\frac{1}{\varepsilon}\mathrm{Tr}(\mathbf{W}_k+\mathbf{R}_{\mathrm{d}})+P_C}, \forall i \in \{t,r\}. \end{cases} \tag{17}$$

2.3.2. Sensing model

We choose the illumination power as the sensing performance metric. Similarly, the signal received by the q-th target is:

$$\begin{aligned} y_q &= \mathbf{h}_q^H \Phi_i \mathbf{G} x + \mathbf{n}_q \\ &= \mathbf{h}_q^H \Phi_i \mathbf{G}\left(\sum_{k\in\mathscr{K}} \omega_k s_k + \mathbf{d}\right) + \mathbf{n}_q, \forall i \in \{t,r\}, \end{aligned} \tag{18}$$

where $n_q \sim \mathscr{CN}\left(0,\sigma_q^2\right)$ denotes the complex AWGN of the q-th target with zero mean and variances σ_q^2. We assume that the communication signals can also be used for detection, so the illumination power of the q-th target can be expressed as:

$$\begin{aligned} P_q^{\mathrm{illu}} &= \mathbb{E}\left[\left|\mathbf{h}_q^H \Phi_i \mathbf{G} x[t]\right|^2\right] \\ &= \mathbf{h}_q^H \Phi_i \mathbf{G}\left(\sum_{k\in\mathscr{K}} \omega_k \omega_k^H + \mathbf{d}\mathbf{d}^H\right)\left(\mathbf{h}_q^H \Phi_i \mathbf{G}\right)^H \\ &= \tilde{\mathbf{h}}_q\left(\sum_{k\in\mathscr{K}} \mathbf{W}_k + \mathbf{R}_{\mathrm{d}}\right)\tilde{\mathbf{h}}_q^H \\ &= \varphi_i^H \mathbf{H}_q\left(\sum_{k\in\mathscr{K}} \mathbf{W}_k + \mathbf{R}_{\mathrm{d}}\right)\mathbf{H}_q^H \varphi_i \\ &= \mathrm{Tr}\left(\left(\sum_{k\in\mathscr{K}} \mathbf{W}_k + \mathbf{R}_{\mathrm{d}}\right)\mathbf{H}_q^H \Psi_i \mathbf{H}_q\right), \forall i \in \{t,r\}, \end{aligned} \tag{19}$$

where $\tilde{\mathbf{h}}_q = \mathbf{h}_q^H \Phi_i \mathbf{G} = \varphi_i^H \mathrm{diag}\left(\mathbf{h}_q^H\right)\mathbf{G} = \varphi_i^H \mathbf{H}_q \in \mathbb{C}^{1\times M}, \mathbf{H}_q = \mathrm{diag}\left(\mathbf{h}_q^H\right)\mathbf{G} \in \mathbb{C}^{N\times M}$ can be seen as the equivalent cascaded channel from DFBS through STAR-RIS to target q.

2.4. Problem formulation

In this paper, we aim to maximize the minimum EE of communication users, as well as satisfying the per-target worst illumination power τ_q constraint, the transmit power budget $P^{\max}$ at DFBS and the STAR-RIS TCs & RCs constraints, via the jointly design with the DFBS transmit beamforming $\{\mathbf{W}_k\}, \forall k$ and $\mathbf{R}_{\mathrm{d}}$, the STAR-RIS reflection beamforming φ_r and transmission beamforming φ_t. The optimization problem thus can be formulated as follows:

$$\mathscr{P}_0: \max_{\{\mathbf{W}_k\},\mathbf{R}_{\mathrm{d}},\Psi_t,\Psi_r,\lambda^t,\lambda^r} \min_{k\in\mathscr{K}} EE_k^{\mathscr{X}} \tag{20a}$$

$$\text{s.t. } \mathrm{C}_1: \begin{cases} P_q^{\mathrm{illu}} \geq \tau_q, \forall q \in \mathscr{Q}, \mathscr{X} \in \{\mathrm{ES,MS}\}, \\ \lambda^i P_q^{\mathrm{illu}} \geq \tau_q, \forall q \in \mathscr{Q}, \mathscr{X} = \mathrm{TS}, \forall i \in \{t,r\}, \end{cases} \tag{20b}$$

$$\mathrm{C}_2: \begin{cases} P_T^{\mathrm{ES/MS}} \leq P^{\max}, \mathscr{X} \in \{\mathrm{ES,MS}\}, \\ P_T^{\mathrm{TS}} \leq P^{\max}, \mathscr{X} = \mathrm{TS}, \end{cases} \tag{20c}$$

$$\mathrm{C}_3: \beta_{i,n} \in \mathscr{A}^{\mathscr{X}}, \forall n \in \mathscr{N}, \forall i \in \{t,r\}, \tag{20d}$$

$$\mathrm{C}_4: \phi_{i,n} \in [0, 2\pi), \forall n \in \mathscr{N}, \forall i \in \{t,r\}, \tag{20e}$$

$$\mathrm{C}_5: \mathbf{W}_k \succeq \mathbf{0}, \mathrm{Rank}(\mathbf{W}_k) = 1, \mathbf{R}_{\mathrm{d}} \succeq \mathbf{0}, \forall k \in \mathscr{K}, \tag{20f}$$

$$\mathrm{C}_6: \Psi_i \succeq \mathbf{0}, \mathrm{Rank}(\Psi_i) = 1, \forall i \in \{t,r\}, \tag{20g}$$

$$\mathrm{C}_7: 0 \leq \lambda^t \leq 1, 0 \leq \lambda^r \leq 1, \lambda^t + \lambda^r = 1, \mathscr{X} = \mathrm{TS}, \tag{20h}$$

where $\mathscr{X} \in \{\mathrm{ES,MS,TS}\}$ refers to the mode employed by STAR-RIS. Constraints C_1 indicates the radar sensing illumination power requirement per target, C_2 represents the given maximum power budget at the DFBS, C_3 and C_4 are the STAR-RIS amplitude and phase shift nature, respectively, C_6 means the rank-one constraint and C_7 indicates the time requirement of TS mode.

One can observe that the main difficulty for solving $\mathscr{P}_0$ is the non-convexity induced by the objective function and highly coupled variables in constraints. To tackle this issue, we propose an efficient iterative algorithm in the next section.

3. Proposed joint beamforming optimization schemes

In this section, we first resolve the optimization problem adopting ES and MS modes, and then solves the problem with TS mode.

3.1. Proposed schemes for ES and MS modes

We apply the AO method to solve $\mathscr{P}_0$ with $\mathscr{X} \in \{\mathrm{ES,MS}\}$, namely optimizing $(\{\mathbf{W}_k\}, \mathbf{R}_{\mathrm{d}})$ and (φ_r, φ_t) alternatively until convergence.

3.1.1. Problem reformulation

Firstly, we introduce an auxiliary variables $\alpha = [\alpha_1, \cdots, \alpha_K]$, and the optimization problem with regard to ES and MS modes can be converted to the following one:

$$\mathscr{P}_1: \max_{\{\mathbf{W}_k\},\mathbf{R}_\mathrm{d},\Psi_t,\Psi_r,\alpha} \min_{k\in\mathscr{K}} \frac{\log_2(1+\alpha_k)}{\frac{1}{\varepsilon}\mathrm{Tr}(\mathbf{W}_k+\mathbf{R}_\mathrm{d})+P_C} \tag{21a}$$

$$\text{s.t. } \mathrm{C}_8: \alpha_k \le \frac{\mathrm{Tr}\left(\mathbf{W}_k\mathbf{H}_k^H\Psi_i\mathbf{H}_k\right)}{\mathrm{Tr}\left(\mathbf{J}_k^{\mathrm{ES/MS}}\mathbf{H}_k^H\Psi_i\mathbf{H}_k\right)+\sigma_k^2}, k\in\mathscr{K}, \tag{21b}$$

$$\mathrm{C}_1: P_q^{\mathrm{illu}} \ge \tau_q, \forall q\in\mathscr{Q}, \tag{21c}$$

$$\mathrm{C}_2: \mathrm{Tr}\left(\sum_{k\in\mathscr{K}}\mathbf{W}_k+\mathbf{R}_\mathrm{d}\right)\le P^{\max}, \tag{21d}$$

$$\mathrm{C}_3: \beta_{i,n}\in\mathscr{A}^{\mathrm{ES/MS}}, \forall n\in\mathscr{N}, \forall i\in\{t,r\}, \tag{21e}$$

$$\mathrm{C}_4, \mathrm{C}_5, \mathrm{C}_6. \tag{21f}$$

Subsequently, so as to streamline the complexity of the formulated max-min problem, an auxiliary variable, denoted as η, is brought in to represent the minimum EE. This transformation enables $\mathscr{P}_1$ to be reformulated into the subsequent equivalent one:

$$\mathscr{P}_{1.1}: \max_{\{\mathbf{W}_k\},\mathbf{R}_\mathrm{d},\Psi_t,\Psi_r,\alpha,\eta} \quad \eta \tag{22a}$$

$$\text{s.t. } \mathrm{C}_9: \frac{\log_2(1+\alpha_k)}{\frac{1}{\varepsilon}\mathrm{Tr}(\mathbf{W}_k+\mathbf{R}_\mathrm{d})+P_C} \ge \eta, k\in\mathscr{K}, \tag{22b}$$

$$\mathrm{C}_1, \mathrm{C}_2, \mathrm{C}_3, \mathrm{C}_4, \mathrm{C}_5, \mathrm{C}_6, \mathrm{C}_8. \tag{22c}$$

In the following, the AO method is adopted to divide $\mathscr{P}_{1.1}$ into two sub-problem.

3.1.2. Fix TCs & RCs and solve $(\{\mathbf{W}_k\},\mathbf{R}_\mathrm{d})$

For given TCs & RCs of STAR-RIS, *i.e.*, (φ_r,φ_t), the sub-problem with respect to $(\{\mathbf{W}_k\},\mathbf{R}_\mathrm{d})$ can be expressed as:

$$\mathscr{P}_2: \max_{\{\mathbf{W}_k\},\mathbf{R}_\mathrm{d},\alpha,\eta} \quad \eta \tag{23a}$$

$$\text{s.t. } \mathrm{C}_1, \mathrm{C}_2, \mathrm{C}_5, \mathrm{C}_8, \mathrm{C}_9. \tag{23b}$$

It is obvious that due to the non-convex of the constraints, it is difficult to directly solve the above problem. Therefore, we first use the FP method to equivalently convert the fractional constraints C_9 into the subtraction form [40]. By introducing auxiliary variables $\rho=[\rho_1,\cdots,\rho_K]$, C_9 can be rewritten as:

$$\tilde{\mathrm{C}}_9: f(\alpha_k,\rho_k)=2\rho_k\sqrt{\log_2(1+\alpha_k)}-\rho_k^2\left(\frac{1}{\varepsilon}\mathrm{Tr}(\mathbf{W}_k+\mathbf{R}_\mathrm{d})+P_C\right)\ge\eta, \forall k\in\mathscr{K}, \tag{24}$$

Thus, given other variables, the optimal value of the auxiliary variable ρ can be obtained by setting $\frac{\partial f(\alpha_k,\rho_k)}{\rho_k}=0$:

$$\rho_k^{\mathrm{opt}}=\frac{\sqrt{\log_2\left(1+\alpha_k^{[l]}\right)}}{\frac{1}{\varepsilon}\mathrm{Tr}\left(\mathbf{W}_k^{[l]}+\mathbf{R}_\mathrm{d}^{[l]}\right)+P_C}, \forall k\in\mathscr{K}, \tag{25}$$

where $[l]$ denotes the value at the l-th iteration. After obtaining ρ, $\mathscr{P}_2$ is still intractable due to the non-convex constraints C_8 and C_5. To this end, by introducing auxiliary variables $\delta=[\delta_1,\ldots,\delta_K]\in\mathbb{R}^K$ and $\chi=[\chi_1,\ldots,\chi_K]\in\mathbb{R}^K$, C_8 can be transformed into:

$$\mathrm{C}_{10}: \delta_k \leq \mathrm{Tr}\left(\mathbf{W}_k \mathbf{H}_k^H \Psi_i \mathbf{H}_k\right), \forall k \in \mathscr{K}, \tag{26a}$$

$$\mathrm{C}_{11}: \alpha_k \chi_k \leq \delta_k, \forall k \in \mathscr{K}, \tag{26b}$$

$$\mathrm{C}_{12}: \chi_k \geq \mathrm{Tr}\left(\mathbf{J}_k^{\mathrm{ES/MS}} \mathbf{H}_k^H \Psi_i \mathbf{H}_k\right) + \sigma_k^2, \forall k \in \mathscr{K}. \tag{26c}$$

For C_{11}, we can obtain its upper bound as [41,42]:

$$\frac{\alpha_k^{[l]}}{2\chi_k^{[l]}}\chi_k^2 + \frac{\chi_k^{[l]}}{2\alpha_k^{[l]}}\alpha_k^2 \geq \alpha_k \chi_k, \forall k \in \mathscr{K}, \tag{27}$$

where $\alpha_k^{[l]}$ and $\chi_k^{[l]}$ are the values of α_k and χ_k at the l-th iteration, respectively. Thus, C_{11} can be rewritten as:

$$\tilde{\mathrm{C}}_{11}: \frac{\alpha_k^{[l]}}{2\chi_k^{[l]}}\chi_k^2 + \frac{\chi_k^{[l]}}{2\alpha_k^{[l]}}\alpha_k^2 \leq \delta_k, \forall k \in \mathscr{K}. \tag{28}$$

Through the above series of transformations, $\mathscr{P}_2$ can be transformed as:

$$\mathscr{P}_{2.1}: \max_{\{\mathbf{W}_k\}, \mathbf{R}_\mathrm{d}, \alpha, \delta, \chi, \eta} \eta \tag{29a}$$

$$\text{s.t. } \mathrm{C}_1, \mathrm{C}_2, \mathrm{C}_5, \tilde{\mathrm{C}}_9, \mathrm{C}_{10}, \tilde{\mathrm{C}}_{11}, \mathrm{C}_{12}. \tag{29b}$$

It can be observed that the non-convexity of $\mathscr{P}_{2.1}$ lies in the rank-one constraint of C_5, except for it, the other parts are solvable convex constraints. To this end, we can employ SDR technique to ignore the rank-one constraint and solve the relaxed problem by SDP technique. After obtaining the solution, the Gaussian randomization or eigenvalue decomposition method can be used to construct the rank-one solution.

3.1.3. Fix $(\{\mathbf{W}_k\}, \mathbf{R}_\mathrm{d})$ and solve TCs & RCs

For given $(\{\mathbf{W}_k\}, \mathbf{R}_\mathrm{d})$, the sub-problem with respect to (φ_r, φ_t) can be expressed as:

$$\mathscr{P}_3: \max_{\Psi_t, \Psi_r, \alpha, \delta, \chi, \eta} \eta \tag{30a}$$

$$\text{s.t. } \mathrm{C}_1, \mathrm{C}_4, \mathrm{C}_6, \tilde{\mathrm{C}}_9, \mathrm{C}_{10}, \tilde{\mathrm{C}}_{11}, \mathrm{C}_{12}, \tag{30b}$$

$$\mathrm{C}_3: \beta_{i,n} \in \mathscr{A}^{\mathrm{ES/MS}}, \forall n \in \mathscr{N}, \forall i \in \{t, r\}. \tag{30c}$$

However, the rank-one constraint C_6 and the binary constraint C_3 for MS mode are still non-convex. Next, the penalty-based algorithm is adopted to solve the optimization problem under ES mode and MS mode.

3.1.4. Penalty-based algorithm for ES mode

The rank-one constraint C_6 can be rewritten as the following equivalent form [43]:

$$\mathrm{Rank}\left(\Psi_i\right) = 1 \Leftrightarrow \|\Psi_i\|_* - \|\Psi_i\|_2 = 0, \forall i \in \{t, r\}, \tag{31}$$

where $\|\Psi_i\|_* = \sum_j \sigma_j\left(\Psi_i\right)$ and $\|\Psi_i\|_2 = \sigma_1\left(\Psi_i\right)$ refer to the nuclear norm and the spectral norm of Ψ_i, respectively, and $\sigma_j\left(\Psi_i\right)$ is the j-th largest singular value of matrix Ψ_i. Since for any $\Psi_i \in \mathbb{H}^M$ and $\Psi_i \succeq 0$, there is always $\|\Psi_i\|_* - \|\Psi_i\|_2 \geq 0$, the equality holds if and only if Ψ_i satisfies the rank-one constraint. Therefore, we can replace C_6 with Equation (31). Then, the penalty-based method is used to solve

problem $\mathscr{P}_3$. Concretely, by leveraging the above transformation and adding constraint (Equation (31)) to the objective function as penalty terms, $\mathscr{P}_3$ can be transformed into:

$$\mathscr{P}_{3.1}: \max_{\Psi_t,\Psi_r,\alpha,\delta,\chi,\eta} \eta - v \sum_{i\in\{t,r\}} (\|\Psi_i\|_* - \|\Psi_i\|_2) \tag{32a}$$

$$\text{s.t. } \mathrm{C}_1, \mathrm{C}_4, \tilde{\mathrm{C}}_9, \mathrm{C}_{10}, \tilde{\mathrm{C}}_{11}, \mathrm{C}_{12}, \tag{32b}$$

$$\mathrm{C}_3: \beta_{r,n} \in [0,1], \beta_{t,n} + \beta_{r,n} = 1, \forall n \in \mathscr{N}, \tag{32c}$$

$$\mathrm{C}_6: \Psi_i \succeq \mathbf{0}, \forall i \in \{t,r\}, \tag{32d}$$

where $v > 0$ is the penalty factor. Please note that when Ψ_i does not satisfy the rank-one condition, the penalty factor will punish the objective function, and the larger value of v, the smaller value of penalty term. But if v starts with a large value, the penalty term will dominate the objective function. Consequently, v should begin with a low value to find an appropriate initial point, and then, v can be incrementally increased to derive feasible solutions for Ψ_i that ultimately meet the rank-one condition. However, since the non-convex nature of the objective function, $\mathscr{P}_{3.1}$ remains challenging to resolve. To address this, SCA method is employed to derive a sub-optimal solution for $\mathscr{P}_{3.1}$. Specifically, in the l-th iteration of the SCA method, for a specified point $\Psi_i^{(l)}$, we utilize the first-order Taylor expansion to establish a convex upper bound for the penalty term:

$$\|\Psi_i\|_* - \|\Psi_i\|_2 \leq \|\Psi_i\|_* - \hat{\Psi}_i^{(l)}, \tag{33}$$

where $\hat{\Psi}_i^{(l)} \triangleq \left\|\Psi_i^{(l)}\right\|_2 + \mathrm{Tr}\left[u_{\max}\left(\Psi_i^{(l)}\right)\left(u_{\max}\left(\Psi_i^{(l)}\right)\right)^H\left(\Psi_i - \Psi_i^{(l)}\right)\right]$ and $u_{\max}\left(\Psi_i^{(l)}\right)$ represents the maximum eigenvector corresponding to $\Psi_i^{(l)}$. Finally, $\mathscr{P}_{3.1}$ can be rewritten as:

$$\mathscr{P}_{3.2}: \max_{\Psi_t,\Psi_r,\alpha,\delta,\chi,\eta} \eta - v \sum_{i\in\{t,r\}} \left(\|\Psi_i\|_* - \hat{\Psi}_i^{(l)}\right) \tag{34a}$$

$$\text{s.t. } \mathrm{C}_1, \mathrm{C}_3, \mathrm{C}_6, \mathrm{C}_4, \tilde{\mathrm{C}}_9, \mathrm{C}_{10}, \tilde{\mathrm{C}}_{11}, \mathrm{C}_{12}. \tag{34b}$$

It is clear that $\mathscr{P}_{3.2}$ is a convex optimization which can be effectively tackled with standard convex optimization algorithm or tools, e.g., CVX, and the obtained result can directly meet the rank-one condition. Thus, similarly, we can apply the eigenvalue decomposition to obtain feasible φ_i^{opt}.

To conclude, a penalty-based algorithm is proposed to solve STAR-RIS optimization with ES mode, which includes two iteration loops. In the outer loop, the penalty factor v is gradually increased according to $v^{(l+1)} = cv^{(l)}$, $c > 1$. In the inner loop, the penalty-based convex optimization is solved, and the termination condition of the inner loop is:

$$\max_{i\in\{r,t\}} \{\|\Psi_i\|_* - \|\Psi_i\|_2\} \leq \varepsilon_1. \tag{35}$$

3.1.5. Extended penalty-based algorithm for MS mode

Compared with the ES mode, the difference between them lies in C_3 that MS owns an additional non-convex binary constraint, *i.e.*, $\beta_{i,n} \in \{0,1\}, \forall n \in \mathscr{N}, \forall i \in \{t,r\}$. Thus, except for this binary constraint, other constraints can be handled similarly as previously described in ES case. Next, we focus on tackling

this issue through approximating this constraint with the penalty-based method. First, we convert the binary constraint $\beta_{i,n} \in \{0,1\}$ into the following relaxed one [20]:

$$\beta_{i,n} - (\beta_{i,n})^2 \geq 0, \quad \forall n \in \mathcal{N}, \forall i \in \{t,r\}, \tag{36}$$

where equality holds if and only if $\beta_{i,n} \in \{0,1\}$. In the following, by adding the penalty term of binary constraint, the proposed penalty-based algorithm for ES that mentioned-above has been extended to solve the optimization problem for MS. The penalty term is constructed as $\varsigma \sum_{i\in\{t,r\}} \sum_{n\in\mathcal{N}} \left(\beta_{i,n} - (\beta_{i,n})^2\right)$, where $\varsigma > 0$ is the penalty factor. With the first-order Taylor expansion, the convex upper bound for the new binary penalty term can be obtained as:

$$\begin{aligned} \beta_{i,n} - (\beta_{i,n})^2 &\leq \beta_{i,n} - \left(\beta_{i,n}^{[l]}\right)^2 - 2\beta_{i,n}^{[l]}\left(\beta_{i,n} - \beta_{i,n}^{[l]}\right) \\ &= \left(1 - 2\beta_{i,n}^{[l]}\right)\beta_{i,n} + \left(\beta_{i,n}^{[l]}\right)^2 \\ &\triangleq \Pi\left(\beta_{i,n}, \beta_{i,n}^{[l]}\right), \forall n \in \mathcal{N}, \forall i \in \{t,r\}, \end{aligned} \tag{37}$$

where $\beta_{i,n}^{[l]}$ is a given point in the l-th iteration of the SCA method. Therefore, we have:

$$\mathscr{P}_4 : \max_{\Psi_t,\Psi_r,\alpha,\delta,\chi,\eta} \eta - v\sum_{i\in\{t,r\}}\left(\|\Psi_i\|_* - \hat{\Psi}_i^{[l]}\right) - \varsigma\sum_{i\in\{t,r\}}\sum_{n\in\mathcal{N}}\Pi\left(\beta_{i,n},\beta_{i,n}^{[l]}\right) \tag{38a}$$

$$\text{s.t. } \mathrm{C}_1, \mathrm{C}_4, \mathrm{C}_6, \tilde{\mathrm{C}}_9, \mathrm{C}_{10}, \tilde{\mathrm{C}}_{11}, \mathrm{C}_{12}, \tag{38b}$$

$$\mathrm{C}_3 : \beta_{t,n} + \beta_{r,n} = 1, \forall n \in \mathcal{N}. \tag{38c}$$

It is clearly that $\mathscr{P}_4$ is a convex optimization problem, which can be effectively tackled with standard convex optimization algorithm or tools, e.g., CVX. Similarly, in the outer loop, the penalty factors v and ς are gradually increased according to $v^{[l+1]} = cv^{[l]}$ and $\varsigma^{[l+1]} = c\varsigma^{[l]}$, respectively. In the inner loop, the penalty-based convex optimization is solved, and the termination condition of the inner loop is:

$$\max_{i\in\{r,t\}}\left(\|\Psi_i\|_* - \|\Psi_i\|_2, \beta_{i,n} - (\beta_{i,n})^2\right) \leq \varepsilon_2. \tag{39}$$

The details of the penalty-based algorithm for STAR-RIS optimization under ES and MS modes is summarized in Algorithm 1.

Algorithm 1 Proposed penalty-based algorithm for solving problem $\mathscr{P}_3$

Input: $\mathbf{h}_k$, $\mathbf{h}_q$, $\mathbf{G}$, $P^{\max}$, τ_q, ε_1, ε_2, δ_{th}, DFBS beamforming $\{\mathbf{W}_k\}$ and $\mathbf{R}_{\mathrm{d}}$.
Output: STAR-RIS RCs Φ_r and TCs Φ_t.
1: Initialize: $\Phi_{t/r}$, $R = 0$, the penalty factors $v^0 = 0$ and $\varsigma^0 = 0$.
2: **repeat: outer loop**
3: Set the inner iteration index $l = 0$;
4: **repeat: inner loop**
5: For fixed $\{\mathbf{W}_k\}$ and $\mathbf{R}_{\mathrm{d}}$, optimize $\Psi_r^{(l)}$, $\Psi_t^{(l)}$ by solving $\mathscr{P}_{3.2}$ for ES mode and $\mathscr{P}_4$ for MS mode;
6: Update $\Psi_r^{(l+1)}$ and $\Psi_t^{(l+1)}$ with the obtained optimal solutions, and $l = l + 1$;
7: **until** The maximum variation of all penalty terms (Equations (35) and (39)) are below the predefined threshold ε_1 and ε_2, respectively;
8: Update the penalty factors $v = cv$ and $\varsigma = c\varsigma$;
9: **until** The relevant variation of objective value for $\mathscr{P}_3$ is below a predefined threshold δ_{th}.

Summarily, to solve $\mathscr{P}_1$, we first initialize the feasible variables $\{\mathbf{W}_k\}$, $\mathbf{R}_\mathrm{d}$, φ_t and φ_r, and solve $\mathscr{P}_{2.1}$ to obtain $\left\{\mathbf{W}_k^{\mathrm{opt}}\right\}$ and $\mathbf{R}_\mathrm{d}^{\mathrm{opt}}$, hereafter, solve $\mathscr{P}_3$ to obtain Ψ_r^{opt} and Ψ_t^{opt}, then, repeat $\mathscr{P}_{2.1}$ and $\mathscr{P}_3$ until the value of EE converges to a stable value, which is summarized as Algorithm 2.

Algorithm 2 Joint beamforming design for STAR-RIS-aided near-field ISAC system under ES/MS modes

Input: $\mathbf{h}_k$, $\mathbf{h}_q$, $\mathbf{G}$, $P^{\max}$, τ_q, ε_1, ε_2, δ_{th}.
Output: DFBS beamforming $\{\mathbf{W}_k\}$ and $\mathbf{R}_\mathrm{d}$, STAR-RIS RCs Φ_r and TCs Φ_t.
1: Initialize: $\{\mathbf{W}_k\}$, $\mathbf{R}_\mathrm{d}$, $\Phi_{t/r}$, $i=1$, $\delta=\infty$, $\eta=0$.
2: **while** $i \le \Gamma_{\max}$ and $\delta \ge \delta_{th}$ **do**
3: $\quad \mathscr{P}_{\mathrm{pre}} = \eta$;
4: $\quad$ Optimize $\{\mathbf{W}_k\}$ and $\mathbf{R}_\mathrm{d}$ by solving $\mathscr{P}_{2.1}$;
5: $\quad$ Optimize Ψ_r and Ψ_t by Algorithm 1;
6: $\quad$ Calculate EE_k by (17) and $\mathscr{P}_{\mathrm{EE}} = \min(EE_k)$;
7: $\quad \delta = \frac{\left|\mathscr{P}_{\mathrm{pre}} - \mathscr{P}_{\mathrm{EE}}\right|}{\mathscr{P}_{\mathrm{EE}}}$;
8: $\quad i = i+1$.
9: **end while**

3.2. Proposed scheme for TS mode

When adopting the TS mode, the STAR-RIS TCs and RCs for allocation time λ^i is $\varphi_i = \left[e^{j\phi_{i,1}}, e^{j\phi_{i,2}}, \ldots, e^{j\phi_{i,N}}\right]^T \in \mathbb{C}^{N\times 1}$, $\forall i \in \{t,r\}$, and $\Psi_i = \varphi_i \varphi_i^H$ should satisfy $\mathrm{diag}(\Psi_i) = \mathbf{I}_N$, $\forall i \in \{t,r\}$, which means the TCs & RCs are not coupled. Note that, in the following parts, $\forall i \in \{t,r\}$, unless otherwise specified. Thus, the optimization problem can be expressed as:

$$\mathscr{P}_5: \max_{\{\mathbf{W}_k\},\mathbf{R}_\mathrm{d},\Psi_t,\Psi_r,\lambda^t,\lambda^r} \min_{k\in\mathscr{K}} \frac{\lambda^i \log_2\left(1+\mathrm{SINR}_{k,i}^{\mathrm{TS}}\right)}{\frac{1}{\varepsilon}\mathrm{Tr}\left(\mathbf{W}_k+\mathbf{R}_\mathrm{d}\right)+P_C} \tag{40a}$$

$$\text{s.t. } \mathrm{C}_1: \lambda^i P_q^{\mathrm{illu}} \ge \tau_q, \forall q \in \mathscr{Q}, \tag{40b}$$

$$\mathrm{C}_2: P_T^{\mathrm{TS}} \le P^{\max}, \tag{40c}$$

$$\mathrm{C}_3: \beta_{t,n}=1, \beta_{r,n}=1, \forall n \in \mathscr{N}, \tag{40d}$$

$$\mathrm{C}_4, \mathrm{C}_5, \mathrm{C}_7, \tag{40e}$$

$$\mathrm{C}_6: \Psi_i \succeq \mathbf{0}, \mathrm{Rank}(\Psi_i)=1, \mathrm{diag}(\Psi_i)=\mathbf{I}_N. \tag{40f}$$

Similar to ES, by introducing auxiliary variable $\alpha = [\alpha_1, \ldots, \alpha_K]$, $\mathscr{P}_5$ can be converted into:

$$\mathscr{P}_{5.1}: \max_{\{\mathbf{W}_k\},\mathbf{R}_\mathrm{d},\Psi_t,\Psi_r,\lambda^t,\lambda^r,\alpha} \min_{k\in\mathscr{K}} \frac{\lambda^i \log_2(1+\alpha_k)}{\frac{1}{\varepsilon}\mathrm{Tr}\left(\mathbf{W}_k+\mathbf{R}_\mathrm{d}\right)+P_C} \tag{41a}$$

$$\text{s.t. } \mathrm{C}_8: \alpha_k \le \frac{\mathrm{Tr}\left(\mathbf{W}_k \mathbf{H}_k^H \Psi_i \mathbf{H}_k\right)}{\mathrm{Tr}\left(\mathbf{J}_k^{\mathrm{TS}} \mathbf{H}_k^H \Psi_i \mathbf{H}_k\right)+\sigma_k^2}, \forall k \in \mathscr{K}, \tag{41b}$$

$$\mathrm{C}_1, \mathrm{C}_2, \mathrm{C}_3, \mathrm{C}_4, \mathrm{C}_5, \mathrm{C}_6, \mathrm{C}_7, \tag{41c}$$

Then, convert the max-min problem into:

$$\mathscr{P}_{5.2}: \max_{\{\mathbf{W}_k\},\mathbf{R}_\mathrm{d},\Psi_t,\Psi_r,\lambda^t,\lambda^r,\alpha,\eta} \quad \eta \tag{42a}$$

$$\text{s.t. } \mathrm{C}_9: \frac{\log_2(1+\alpha_k)}{\frac{1}{\varepsilon}\mathrm{Tr}\left(\mathbf{W}_k+\mathbf{R}_\mathrm{d}\right)+\frac{P_C}{\lambda^i}} \ge \eta, \forall k \in \mathscr{K}, \tag{42b}$$

$$\mathrm{C}_1, \mathrm{C}_2, \mathrm{C}_3, \mathrm{C}_4, \mathrm{C}_5, \mathrm{C}_6, \mathrm{C}_7, \mathrm{C}_8. \tag{42c}$$

Similarly, we first introduce auxiliary variables $\rho = [\rho_1, \ldots, \rho_K]$, and use the FP method to transform C_9 into:

$$\tilde{C}_9 : f\left(\alpha_k, \rho_k, \lambda^i\right) = 2\rho_k \sqrt{\lambda^i \log_2\left(1+\alpha_k\right)} - \rho_k^2 \left(\frac{1}{\varepsilon}\mathrm{Tr}\left(\mathbf{W}_k + \mathbf{R}_\mathrm{d}\right) + P_C\right) \geq \eta, \forall k \in \mathscr{K}. \tag{43}$$

Thus, given other variables, the auxiliary variable $\rho = [\rho_1, \ldots, \rho_K]$ can be obtained by:

$$\rho_k^{\mathrm{opt}} = \frac{\sqrt{\lambda^i \log_2\left(1+\alpha_k^{[l]}\right)}}{\frac{1}{\varepsilon}\mathrm{Tr}\left(\mathbf{W}_k^{[l]} + \mathbf{R}_\mathrm{d}^{[l]}\right) + P_C}, \forall k \in \mathscr{K}, \tag{44}$$

where $[l]$ denotes the value at the l-th iteration. Due to C_8 is the same as ES/MS, so its transformation is also the same. Therefore, $\mathscr{P}_{5.2}$ can be rewritten as:

$$\mathscr{P}_{5.3}: \max_{\{\mathbf{W}_k\}, \mathbf{R}_\mathrm{d}, \Psi_t, \Psi_r, \lambda^t, \lambda^r, \eta} \quad \eta \tag{45a}$$

$$\text{s.t. } C_1, C_2, C_3, C_4, C_5, C_6, C_7, \tilde{C}_9, C_{10}, \tilde{C}_{11}, C_{12}. \tag{45b}$$

Next, we use the AO framework to iteratively solve $\mathscr{P}_{5.3}$ until convergence. It can be seen that the solution under TS mode is similar to ES, except that some parameters contain time factors, and thus an additional time factors optimization needs to be added. The solution for $\{\lambda_t, \lambda_r\}$ is as follows:

$$\mathscr{P}_{5.4}: \max_{\lambda^t, \lambda^r, \eta} \quad \eta \tag{46a}$$

$$\text{s.t. } C_1, C_2, C_7, \tilde{C}_9. \tag{46b}$$

Obviously, the above optimization problem is convex and can be solved directly using CVX tools. The details of the optimization algorithm under TS mode is summarized in Algorithm 3.

Algorithm 3 Joint beamforming design for STAR-RIS-aided near-field ISAC system under TS mode

Input: $\mathbf{h}_k$, $\mathbf{h}_q$, $\mathbf{G}$, $P^{\max}$, τ_q, ε_1, δ_{th}.
Output: DFBS beamforming $\{\mathbf{W}_k\}$ and $\mathbf{R}_\mathrm{d}$, STAR-RIS RCs Φ_r and TCs Φ_t, time factors λ_r and λ_t.
1: Initialize: $\{\mathbf{W}_k\}$, $\mathbf{R}_\mathrm{d}$, $\Phi_{t/r}$, $\lambda_{t/r}$, $i = 1$, $\delta = \infty$, $\eta = 0$.
2: **while** $i \leq \Gamma_{\max}$ and $\delta \geq \delta_{th}$ **do**
3: $\quad \mathscr{P}_{\mathrm{pre}} = \eta$;
4: $\quad$ Optimize $\{\mathbf{W}_k\}$ and $\mathbf{R}_\mathrm{d}$ by solving $\mathscr{P}_{2.1}$;
5: $\quad$ Optimize Ψ_r and Ψ_t by Algorithm 1;
6: $\quad$ Optimize λ_r and λ_t by solving $\mathscr{P}_{5.4}$;
7: $\quad$ Calculate EE_k by (17) and $\mathscr{P}_{\mathrm{EE}} = \min(EE_k)$;
8: $\quad \delta = \frac{\left|\mathscr{P}_{\mathrm{pre}} - \mathscr{P}_{\mathrm{EE}}\right|}{\mathscr{P}_{\mathrm{EE}}}$;
9: $\quad i = i + 1$.
10: **end while**

3.3. Analysis of computational complexity

Next, we provide a concise analysis of the computional complexity. Let Δ be the iteration precision, thus, the number of iterations necessary for Algorithm 2 and Algorithm 3 to achieve convergence can be expressed as $\log(\frac{1}{\Delta})$. Firstly, for the Algorithm 2, in each iteration, given the complexity of

finding a solution for the SDR problem, the computational complexity of optimizing DFBS transmit beamforming $(\{\mathbf{W}_k\},\mathbf{R}_{\mathrm{d}})$ is $\mathscr{O}\left(\max\{M,K+Q\}^4\sqrt{M}\right)$. Besides, the main complexity of optimizing STAR-RIS TCs & RCs is caused by solving $\mathscr{P}_{3.2}$ and $\mathscr{P}_4$, which can be expressed as $\mathscr{O}\left(I_{\mathrm{out}}\, I_{\mathrm{in}}\, 2N^{3.5}\right)$, where I_{out} and I_{in} refer to the number of outer and inner iterations required for convergence, respectively, and here we have $I_{\mathrm{out}} = \log(\frac{1}{\Delta})$. Thus, the overall computational complexity of Algorithm 2 is $\mathscr{O}\left(\log(\frac{1}{\Delta})\left(\max\{M,K+Q\}^4\sqrt{M}+I_{\mathrm{in}}\, 2N^{3.5}\right)\right)$. While for Algorithm 3, compared with Algorithm 2, the algorithm design only adds time factor λ^r & λ^t optimization, which is a standard linear convex optimization with a complexity of $\mathscr{O}\left(2^{3.5}\right)$, Thus, the overall computational complexity of Algorithm 3 can be calculated as $\mathscr{O}\left(\log(\frac{1}{\Delta})\left(\max\{M,K+Q\}^4\sqrt{M}+I_{in}2^{3.5}+2^{3.5}\right)\right)$.

4. Numerical results

This section conducts simulation results aimed at evaluating the efficacy of the proposed schemes. The software system used for the simulation is Windows 11 64-bit, with MATLAB R2022a. The hardware specifications used for the simulation are as follows: the CPU is an Intel(R) Core(TM) i7-13700KF CPU @ 3.40 GHz, RAM is 16 GB. For ease of understanding, a three-dimensional coordinate system is utilized to precisely represent the positions of the DFBS and the STAR-RIS. Concretely, the STAR-RIS is positioned at the origin $(0,0,0)$ meters (m), closer to users and targets, while the DFBS is 5 m away from STAR-RIS with a plane coordinate $(0,5,0)$ m and its antennas is set to $M = 6$. We assume that the STAR-RIS operate at a frequency of 10 GHz with $N = 20$, and its antenna aperture is set to $D = 0.2$ m, leading to a near-field region with a Rayleigh distance of 2.6 m. To generate the near-field channels, both users and targets are randomly distributed in the near-field region of STAR-RIS, and the number of users and targets are $K = 4$ and $Q = 4$, respectively, and there are two users and targets on both the r-space and t-space. We set the transmit power and PA efficiency of DFBS to $P^{\max} = 32$ dBm and $\varepsilon = 1/3$, respectively. For simplicity, we set all noise power and minimum target illumination power threshold as the same, *i.e.*, $\sigma_k^2 = \sigma_q^2 = \sigma^2 = -110$ dBm, $\forall k$, $\forall q$, $\tau_q = \tau = -20$ dB, $\forall q$. Besides, for DFBS-STAR-RIS far-field channel, the complex channel gain γ_l for all path is given by $\gamma_l = \sqrt{L_0\left(\frac{d_{BR}}{d_0}\right)^{-\tau_{BR}}}$, where L_0 represents the path loss of the reference distance $d_0 = 1$ m, d_{BR} is the distance between the DFBS and the STAR-RIS, and τ_{BR} denotes the corresponding path loss exponents. The precise parameter configurations are detailed in Table 2. Unless specified otherwise, the aforementioned settings are presumed to be consistently applied throughout our simulation processes.

Table 2. System parameters.

Paramater	Value
The number of DFBS antennas	$M = 6$
The number of STAR-RIS elements	$N = 20$
The number of users	$K = 4$
The number of targets	$Q = 4$
Path loss exponents	$\tau_{BR} = 1.6$
The path loss at 1 m	$L_0 = 30$ dB
Transmit power at the DFBS	$P^{\max} = 32$ dBm
Hardware-dissipated power	$P_{DFBS} = 100$ mW, $P_{STAR-RIS} = 1$ mW, $P_{User} = 10$ mW
The noise power	$\sigma^2 = -110$ dBm
The minimum target illumination power threshold	$\tau = -20$ dB

To verify the effectiveness of our proposed schemes, we conduct a comparison with the following baselines:

- The random phase shift scheme (legend "Random phase STAR-RIS"): Within this scheme, the initial phase shifts of the STAR-RIS, specifically the TCs and RCs, are assigned randomly. The focus of optimization is solely on the design of the DFBS beamforming.
- The conventional RIS scheme (legend "Conventional RIS"): Within this scheme, we assume the utilization of two conventional RISs: one solely designed for reflection and the other exclusively for transmission, each equipped with $N/2$ elements. Note that both are positioned adjacent to each other at the same locale as the STAR-RIS, ensuring a fair basis for comparison. Based on this, the $N/2$ elements work in R status with the RCs are fixed to $\Phi_r = \text{diag}\left(\mathbf{0}_{1\times N/2}, e^{j\phi_{r,1}}, \ldots, e^{j\phi_{r,N/2}}\right)$, and $N/2$ elements work in T status with the TCs are fixed to $\Phi_t = \text{diag}\left(e^{j\phi_{t,1}}, \ldots, e^{j\phi_{t,N/2}}, \mathbf{0}_{1\times N/2}\right)$ [26–29]. Therefore, this scheme can be solved by Algorithm 2, only the settings of TCs and RCs are different.

(1) Relationship between EE and the number of iterations: Figure 3 illustrates the convergence behavior of all considered schemes, including the proposed STAR-RIS schemes operating in three different modes, the conventional RIS-assisted scheme, and the random phase shift scheme. It can be observed that, for all schemes, the EE initially increases with the number of iterations and then gradually approaches a stable value. In particular, the EE converges within approximately 12 iterations, indicating that the proposed iterative optimization algorithm is capable of reaching a steady solution with a relatively small number of iterations. This result verifies both the fast convergence property and the computational efficiency of the proposed algorithm. Furthermore, by comparing the steady-state EE values achieved by different schemes, it is evident that the proposed scheme under the STAR-RIS ES mode attains the highest EE among all considered approaches. This performance advantage mainly stems from the fact that the ES mode provides greater design flexibility and higher DoF in controlling the reflected and transmitted signals. As a result, the ES mode can more effectively exploit the spatial resources provided by STAR-RIS, thereby achieving superior energy efficiency performance compared with the other schemes.

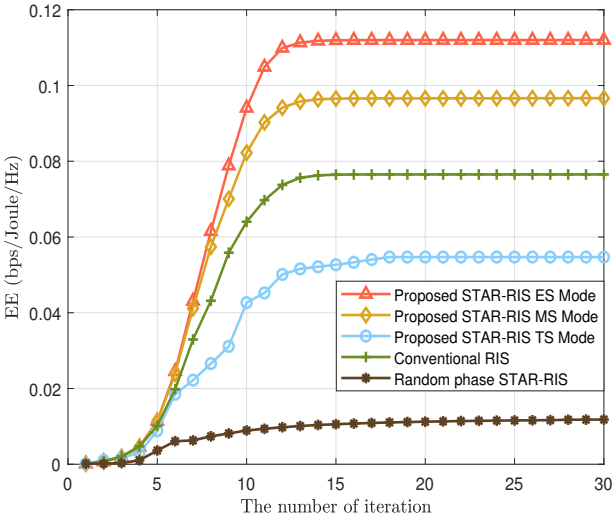

Figure 3. EE versus the number of iterations.

(2) Relationship between EE and DFBS transmit power: Figure 4 provides the relationship between EE and the maximum transmit power $P^{\max}$ under the proposed schemes and the baseline schemes. One

can note that the EE first increases rapidly with the maximum DFBS transmit power under all schemes, and then presents a slow upward trend when the power exceeds 48 dBm, which is easy to understand. Increased transmission power can enhance the beamforming gain for signal transmission, which in turn elevates the overall system performance. While the reason why the rise gradually slows down when the transmit power is relative high lies in the fact that if the power is insufficient, the EE increment is gradual, but once the power reaches saturation, the EE maintains its stability. Furthermore, we observe that the proposed scheme with ES mode outperforms all other schemes. This implies that, when subjected to the stringent requirements of concurrently satisfying both sensing and communication constraints, the ES scheme notably demands less power $P^{\max}$ compared to other schemes, which further confirms that STAR-RIS in ES mode has the highest flexibility in dynamically allocating reflection and transmission resources, thereby achieving the best performance.

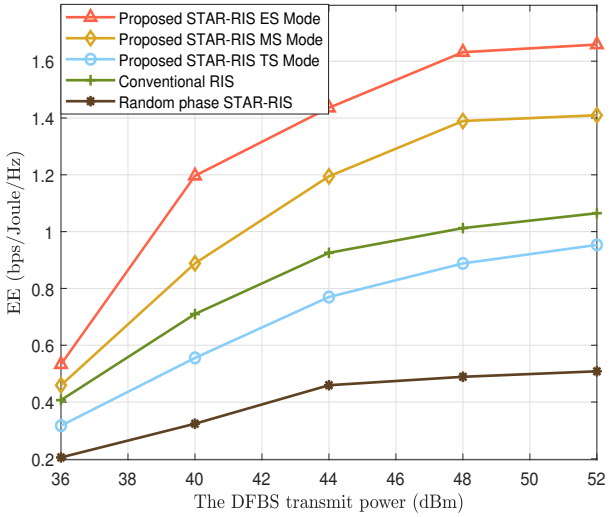

Figure 4. EE versus the DFBS transmit power $P^{\max}$.

(3) EE versus the minimum target illumination power threshold: We plot Figure 5 to show the EE versus the target illumination power threshold τ across all schemes. It can be observed that the EE achieved by all schemes gradually decreases as the sensing requirement τ increases. This trend is expected because a larger target illumination power threshold requires more transmit power to be allocated toward illuminating the targets in order to satisfy the sensing constraints. Consequently, fewer power resources remain available for communication transmission, which leads to a degradation in communication efficiency and ultimately results in a reduction of the overall EE. In addition, this phenomenon clearly reflects the intrinsic trade-off between communication efficiency and sensing performance under limited system resources. Specifically, when more resources are devoted to satisfying stringent sensing requirements, the communication performance inevitably deteriorates. Conversely, prioritizing communication transmission may weaken the sensing capability. Therefore, achieving a proper balance between communication and sensing tasks becomes a critical design consideration for ISAC systems.

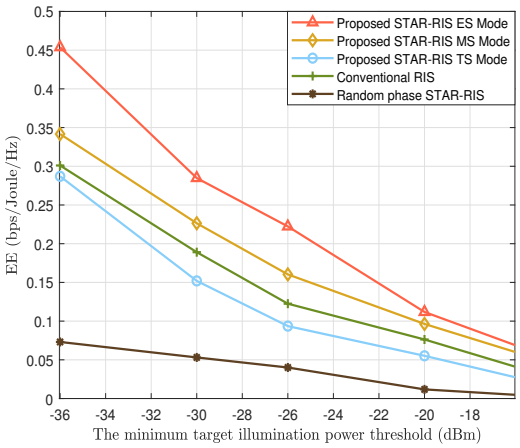

Figure 5. EE versus the minimum target illumination power threshold τ (dBm).

(4) Relationship between EE and the number of STAR-RIS elements: Figure 6 illustrates the variation of EE with respect to the number of STAR-RIS elements under all considered schemes. It can be clearly observed that the EE consistently increases as the number of STAR-RIS elements N grows. This improvement can be attributed to the fact that a larger number of STAR-RIS elements provides greater spatial manipulation capability for the wireless propagation environment. Specifically, with more elements available, the STAR-RIS can more flexibly adjust the reflection and transmission coefficients to construct more favorable channel conditions, thereby enhancing the passive beamforming gain for both communication users and sensing targets. Moreover, the schemes that perform STAR-RIS optimization significantly outperform the random phase shift scheme. This observation highlights the effectiveness of the proposed joint beamforming optimization framework, which jointly designs the DFBS transmit beamforming and STAR-RIS coefficients to better exploit the spatial degrees of freedom offered by the reconfigurable surface. Furthermore, among all considered schemes, the proposed scheme operating under the ES mode achieves the highest EE. This is because the ES mode enables all STAR-RIS elements to be flexibly configured for simultaneous transmission and reflection, thereby providing a higher DoF compared with other operating modes. As a result, the ES mode can more efficiently utilize the available spatial resources, leading to a noticeable performance gap between the proposed scheme and the other benchmark schemes.

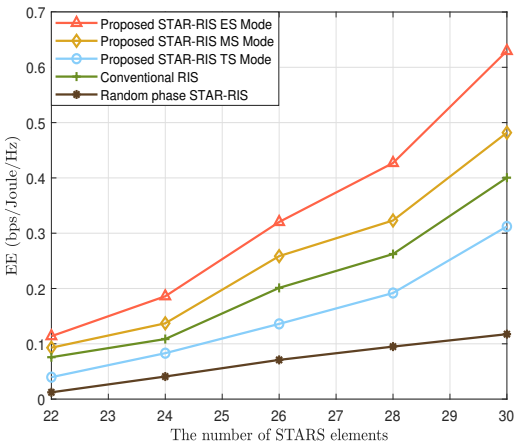

Figure 6. EE versus the number of STAR-RIS elements N.

(5) Relationship between the amplitude of each STAR-RIS element and the target illumination power threshold: Finally, we provide an analysis of the impact of different target illumination power thresholds on the amplitude of STAR-RIS amplitude. To achieve this goal, we assume that all users are located at the r-space, while all targets are located at the other side. As illustrated in Figure 7, each element of STAR-RIS element is capable of modifying the incoming signal in accordance with its specific propagation conditions, and the total of the squared amplitude of reflection and transmission for each STAR-RIS element satisfies $\beta_{r,n}^2 + \beta_{t,n}^2 = 1$. Intuitively, with stricter target illumination power, STAR-RIS needs to allocate a higher proportion of amplitude to the t-space. This allocation strategy is driven by the increased sensing needs, especially when the parameter τ is larger, which encourages the STAR-RIS to introduce more energy resources into the t-space for sensing enhancement.

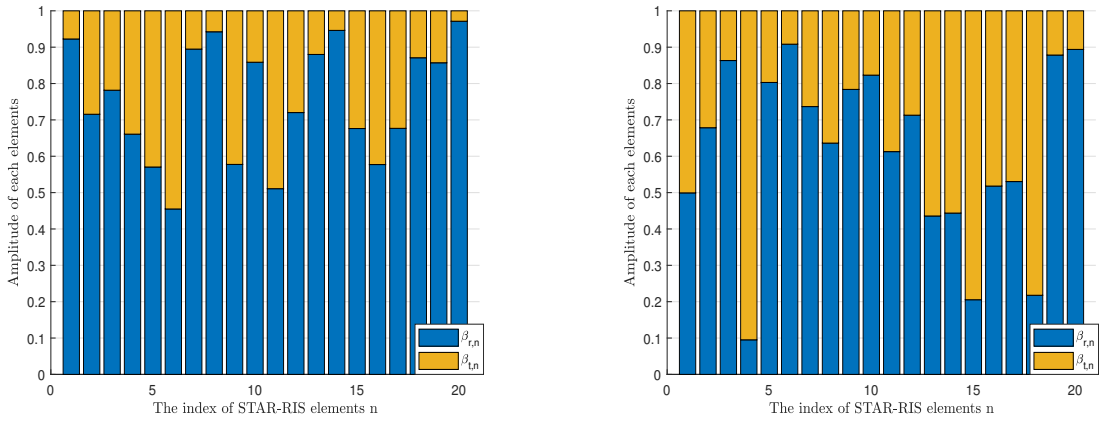

(a) (b)

Figure 7. The amplitude of each STAR-RIS element under different communication thresholds. **(a)** $\gamma = -16$ dB; **(b)** $\gamma = 2$ dB.

5. Conclusion

This paper studied the communication EE optimization problem in the STAR-RIS-aided near-field ISAC system. To guarantee fairness among communication users, we constructed a non-convex optimization framework that jointly optimized the DFBS transmission and STAR-RIS beamforming, with the objective of maximizing the minimum communication EE while satisfying sensing requirements, system transmission power, and STAR-RIS hardware constraints. Specifically, we analyzed the differences among the three modes of STAR-RIS and formulated the max-min EE optimization problem separately under each of these modes. Then, we restructured the optimization problem into an equivalent maximization optimization problem and decomposed it into several sub-problems based on the AO method for alternating solutions until convergence. Concurrently, we analyzed the computational complexity of our proposed algorithms. Finally, the potential and superiority of the proposed schemes were confirmed via numerical simulation results. Building upon existing research, and to further enhance the applicability of the system in real-world environments, we will focus in the future on exploring two critical scenarios: imperfect CSI and target mobility. These factors are prevalent in practical wireless sensing and communication systems and will directly impact sensing accuracy, communication reliability, and resource allocation strategies. Through this research, we will conduct a more in-depth analysis of how practical constraints

such as channel errors, Doppler effects, and time-varying characteristics influence system performance. Furthermore, we will design corresponding robust algorithms and adaptive tracking mechanisms to effectively translate theoretical research into practical applications.

Data availability statement

The data or datasets that support the findings of this study are available from the corresponding author upon reasonable request.

Declaration of generative AI and AI-assisted technologies

During the preparation of this manuscript, the authors used generative AI tools only to improve language and readability. The authors take full responsibility for the content of the manuscript.

Acknowledgments

This work was supported by the National Key Research and Development Program of China (No. 2024YFC3306805), by the Natural Science Foundation of Henan (No. 252300421293), by the Natural Science Foundation of China (No. 62471440 and 62571182), by the Program for Science & Technology Innovation Talents in Universities of Henan Province under Grant 24HASTIT038.

Authors' contribution

Shuang Zhang: conceptualization, methodology, investigation, validation, writing—original and draft preparation. Wanming Hao: methodology and writing—reviewing, editing, supervision and funding acquisition. Gangcan Sun: validation, writing—reviewing, supervision and funding acquisition. All authors have read and agreed to the published version of the manuscript.

Conflicts of interest

Wanming Hao holds the position of Editorial Board Member for *Advanced Information and Communication* and has not peer reviewed or made any editorial decisions for this paper.

References

[1] Liu F, Cui Y, Masouros C, Xu J, Han T, *et al.* Integrated sensing and communications: toward dual-functional wireless networks for 6G and beyond. *IEEE J. Sel. Areas Commun.* 2022, 40(6):1728–1767.

[2] Zhang J, Liu F, Masouros C, Heath R, Feng Z, *et al.* An overview of signal processing techniques for joint communication and radar sensing. *IEEE J. Sel. Top. Signal Process.* 2021, 15(6):1295–1315.

[3] Liu F, Masouros C, Petropulu A, Griffiths H, Hanzo L. Joint radar and communication design: applications, state-of-the art, and the road ahead. *IEEE Trans. Commun.* 2020, 68(6):3834–3862.

[4] Renzo MD, Zappone A, Debbah M, Alouini MS, Tretyakov S. Smart radio environments empowered by reconfigurable intelligent surfaces: how it works, state of research, and the road ahead. *IEEE J. Sel. Areas Commun.* 2020, 38(11):2450–2525.

[5] Liu R, Li M, Luo H, Liu Q, Swindlehurst AL. Integrated sensing and communication with reconfigurable intelligent surfaces: opportunities, applications, and future directions. *IEEE Wireless Commun.* 2023, 30(1):50–57.

[6] He Y, Cai Y, Mao H, Yu G. RIS-assisted communication radar coexistence: joint beamforming design and analysis. *IEEE J. Sel. Area Commun.* 2022, 40(7):2131–2145.

[7] Rihan M, Zappone A, Buzzi S. Robust RIS-assisted MIMO communication-radar coexistence: joint beamforming and waveform design. *IEEE Trans. Commun.* 2023, 71(11):6647–6661.

[8] Xing Z, Wang R, Yuan X. Joint active and passive beamforming design for reconfigurable intelligent surface enabled integrated sensing and communication. *IEEE Trans. Commun.* 2023, 71(4):2457–2474.

[9] Liu R, Li M, Swindlehurst AL. Joint beamforming and reflection design for RIS-assisted ISAC systems. In *Proceedings of the 2022 30th European Signal Processing Conference (EUSIPCO)*, Belgrade, Serbia, August 29–September 2, 2022, pp. 997–1001.

[10] Liu R, Li M, Liu Y, Wu Q, Liu Q. Joint transmit waveform and passive beamforming design for RIS-aided DFRC systems. *IEEE J. Sel. Top. Signal Process.* 2022, 16(5):9957–1010.

[11] Li R, Shao X, Sun S, Tao M, Zhang R. Beam scanning for integrated sensing and communication in IRS-aided mmWave systems. In *Proceedings of 2023 IEEE 24th International Workshop on Signal Processing Advances in Wireless Communications (SPAWC)*, Shanghai, China, September 25–28, 2023, pp. 196–200.

[12] Selvan KT, Janaswamy R. Fraunhofer and Fresnel distances: unified derivation for aperture antennas. *IEEE Antennas Propag. Mag.* 2017, 59(4):12–15.

[13] Cui M, Wu Z, Lu Y, Wei X, Dai L. Near-field MIMO communications for 6G: fundamentals, challenges, potentials, and future directions. *IEEE Commun. Mag.* 2023, 61(1):40–46.

[14] Torres AJ, Sanguinetti L, Björnson E. Near-and far-field communications with large intelligent surfaces. *arXiv* 2020, arXiv:2011.13835.

[15] Zhou Z, Gao X, Fang J, Chen Z. Spherical wave channel and analysis for large linear array in LoS conditions. In *Proceedings of the 2015 IEEE Globecom Workshops (GC Wkshps)*, San Diego, USA, December 6–10, 2015, pp. 1–6.

[16] Cui M, Dai L. Channel estimation for extremely large-scale MIMO: far-field or near-field? *IEEE Trans. Commun.* 2022, 70(4):2663–2677.

[17] Lu Y, Dai L. Near-field channel estimation in mixed LoS/NLoS environments for extremely large-scale MIMO systems. *IEEE Trans. Commun.* 2023, 71(6):3694–3707.

[18] Li Y, Mu X, Xu J, Schober R, Hao Y, *et al.* STAR: simultaneous transmission and reflection for 360° coverage by intelligent surfaces. *IEEE Wireless Commun.* 2021, 28(6):102–109.

[19] Cai W, Li M, Liu Y, Wu L, Liu Q. Joint beamforming design for intelligent omni surface assisted wireless communication systems. *IEEE Trans. Wireless Commun.* 2023, 22(2):1281–1297.

[20] Mu X, Liu Y, Guo L, Lin J, Schober R. Simultaneously transmitting and reflecting (STAR) RIS aided

wireless communications. *IEEE Trans. Wireless Commun.* 2022, 21(5):3083–3098.

[21] Song Y, Xu S, Xu R, Ai B. Weighted sum-rate maximization for multi-STAR-RIS-assisted mmWave cell-free networks. *IEEE Trans. Veh. Technol.* 2024, 73(4):5304–5320.

[22] Zhang S, Hao W, Sun G, Huang C, Zhu Z, *et al.* Joint beamforming optimization for active STAR-RIS-assisted ISAC systems. *IEEE Trans. Wireless Commun.* 2024, 23(11):15888–15902.

[23] Zhang S, Hao W, Sun G, Zhu Z, Li X, *et al.* Joint beamforming design for the STAR-RIS-enabled ISAC systems with multiple targets and multiple users. *IEEE Trans. Commun.* 2025, 73(1):693–708.

[24] Luo H, Liu R, Li M, Liu Q. Toward STAR-RIS-empowered integrated sensing and communications: joint active and passive beamforming design. *IEEE Trans. Veh. Technol.* 2023, 72(12):15991–16005.

[25] Wang Z, Mu X, Liu Y. STARS enabled integrated sensing and communications. *IEEE Trans. Wireless Commun.* 2023, 22(10):6750–6765.

[26] Xue L, Wang K, Yang Z, Peng M. Max-min energy-efficiency fair optimization in STAR-RIS assisted communication system. *IEEE Access* 2023, 11:51106–51116.

[27] Sabharwal A, Schniter P, Guo D, Bliss DW, Rangarajan S, *et al.* In-band full-duplex wireless: challenges and opportunities. *IEEE J. Sel. Areas Commun.* 2014, 32(9):1637–1652.

[28] Zhao B, Ouyang C, Zhang X, Liu Y. Downlink and uplink NOMA-ISAC with signal alignment. *IEEE Trans. Wireless Commun.* 2024, 23(10):15322–15338.

[29] Nasser A, Celik A, Eltawil AM. Joint user-target pairing, power control, and beamforming for NOMA-aided ISAC networks. *IEEE Trans. Cognit. Commun. Networking* 2024, 11(1):316–332.

[30] Xu J, Mu X, Liu Y. Exploiting STAR-RISs in near-field communications. *IEEE Trans. Wireless Commun.* 2024, 23(3):2181–2196.

[31] Li H, Liu Y, Mu X, Chen Y, Pan Z. Joint beamforming for STAR-RIS in near-field communications. In *Proceedings of the GLOBECOM 2023–2023 IEEE Global Communications Conference*, Kuala Lumpur, Malaysia, December 4–8, 2024, pp. 625–630.

[32] Hu C, Dai L, Han S, Wang X. Two-timescale channel estimation for reconfigurable intelligent surface aided wireless communications. *IEEE Trans. Commun.* 2021, 69(11):7736–7747.

[33] Wang Z, Liu L, Cui S. Channel estimation for intelligent reflecting surface assisted multiuser communications: framework, algorithms, and analysis. *IEEE Trans. Wireless Commun.* 2020, 19(10):6607–6620.

[34] You C, Zheng B, Zhang R. Channel estimation and passive beamforming for intelligent reflecting surface: discrete phase shift and progressive refinement. *IEEE J. Sel. Areas Commun.* 2020, 38(11):2604–2620.

[35] Zheng B, You C, Zhang R. Intelligent reflecting surface assisted multi-user OFDMA: channel estimation and training design. *IEEE Trans. Wireless Commun.* 2020, 19(12):8315–8329.

[36] Wei L, Huang C, Alexandropoulos GC, Yuen C. Parallel factor decomposition channel estimation in RIS-assisted multi-user MISO communication. *arXiv* 2020, arXiv:2001.09413.

[37] Wang Z, Xu X, Liu Y. Near-field integrated sensing and communications. *IEEE Commun. Lett.* 2023, 27(8):2048–2052.

[38] Arnold O, Richter F, Fettweis G, Blume O. Power consumption modeling of different base station types in heterogeneous cellular networks. In *Proceedings of the Future Network and Mobile Summit*

2010, Florence, Italy, June 16–18, 2010.

[39] Hao W, Li J, Sun G, Huang C, Zeng M, *et al.* Robust security security energy efficiency optimization for RIS-aided cell-free networks with multiple eavesdroppers. *IEEE Trans. Commun.* 2024, 72(12):7401–7416.

[40] Shen K, Yu W. Fractional programming for communication systems—Part I: power control and beamforming. *IEEE Trans. Signal Process.* 2018, 66(10):2616–2630.

[41] Song P, Scutari G, Facchinei F, Lampariello L. D3M: distributed multi-cell multigroup multicasting. In *Proceedings of the 2016 IEEE International Conference on Acoustics, Speech and Signal Processing (ICASSP)*, Shanghai, China, March 20–25, 2016, pp. 3741–3745.

[42] Hao W, Sun G, Zeng M, Chu Z, Zhu Z, *et al.* Robust design for intelligent reflecting surface-assisted MIMO-OFDMA terahertz IoT networks. *IEEE Internet Things J.* 2021, 8(16):13052–13064.

[43] Jiang T, Shi Y. Over-the-air computation via intelligent reflecting surfaces. *Proceedings of the 2019 IEEE Global Communications Conference (GLOBECOM)*, Hawaii, USA, December 9–13, 2019, pp. 1–6.